

SEMIACTIVE DAMPING OF STAY CABLES NEGLECTING SAG*

By Erik A. Johnson,¹ Associate Member, ASCE, Greg A. Baker,²
B.F. Spencer, Jr.,³ Member, ASCE, and Yozo Fujino,⁴ Member, ASCE

ABSTRACT: Stay cables, such as are used in cable-stayed bridges, are prone to vibration due to their low inherent damping characteristics. Transversely-attached passive viscous dampers have been implemented in many bridges to dampen such vibration. Several studies have investigated optimal passive linear viscous dampers; however, even the optimal passive device can only add a small amount of damping to the cable when attached a reasonable distance from the cable/deck anchorage. This paper investigates the potential for improved damping using semiactive devices. The equations of motion of the cable/damper system are derived using an assumed modes approach and a control-oriented model is developed. The control-oriented model is shown to be more accurate than other models and facilitates low-order control designs. The effectiveness of passive linear viscous dampers is reviewed. The response of a cable with passive, active and semiactive dampers is studied. The response with a semiactive damper is found to be dramatically reduced compared to the optimal passive linear viscous damper for typical damper configurations, thus demonstrating the potential benefits using a semiactive damper for absorbing cable vibratory energy.

INTRODUCTION

Long steel cables, such as are used in cable-stayed bridges and other structures, are prone to vibration induced by the structure to which they are connected and by weather conditions. In particular, light-to-moderate wind combined with light-to-moderate rain has been observed to induce significant cable motion in cables of various cable-stayed bridges; this phenomenon is generally termed “rain-wind induced vibration” (*e.g.*, Hikami, 1986; Hikami and Shiraishi, 1988; Matsumoto, 1998; Main and Jones, 1999). The extremely low damping inherent in such cables, typically on the order of a fraction of a percent (Yamaguchi and Fujino, 1998), is insufficient to eliminate this vibration, causing reduced cable and connection life due to fatigue and/or breakdown of corrosion protection (Watson and Stafford, 1988; Poston, 1998), as well as the risk of losing public confidence in such structures.

Several methods have been proposed and/or implemented to mitigate this problem, though each has its limitations (*e.g.*, Yamaguchi and Fujino, 1998). Tying multiple cables together is a sensible approach, but detracts from the aesthetics of the bridge. Changes to cable roughness or other aerodynamic measures have been effective only for certain classes of vibration, are difficult to implement for retrofit, and have disadvantages at high wind velocities. Active transverse and/or axial control of cable vibration (*e.g.*, Fujino *et al.*, 1993; Yamaguchi and Dung, 1992) may require power sources beyond practical limits, given the number of cables on a typical cable-stayed bridge and the isolated locations at which they are often placed. Discrete passive viscous dampers

1. Assoc. Prof., Dept. of Civil Engrg., Univ. of Southern California, Los Angeles, CA 90089. JohnsonE@usc.edu

2. Formerly, Grad. Rsrch. Asst., Dept. of Civil Engrg. & Geo. Sci., Univ. of Notre Dame, IN 46556.

3. Newmark Endowed Chair in Civil Engineering, Univ. of Illinois, Urbana IL 61801 bfs@uiuc.edu

4. Prof., Dept. of Civil Engrg., University of Tokyo, Bunkyo-ku, Tokyo 113, Japan. fujino@bridge.t.u-tokyo.ac.jp

* Minor corrections were made to this document; the last update was 11/16/2006.

A condensed version of this report appears in the ASCE *J. of Engrg. Mech.* (Johnson *et al.*, 2007); when possible, citation should be made to the archival journal paper, not this report.

Key words: smart damping, stay cables, structural control, semiactive dampers, rain-wind induced vibration

attached perpendicular to the cables have been used on a number of bridges, such as the Brotonne Bridge in France (Gimsing, 1983), the Sunshine Skyway Bridge in Florida (Watson and Stafford, 1988) and the Aratsu Bridge in Japan (Yoshimura *et al.*, 1989), though the damper attachment location is typically restricted to be within 5% (of the cable length) from the cable anchorage.

For an attached discrete linear viscous damper, it has been demonstrated (*e.g.*, Kovacs, 1982; Sulekh, 1990; Pacheco *et al.*, 1993; Krenk, 2000) that an optimal damper size exists for a given cable configuration. This is easily understood when one considers that approaching a zero damping constant in the viscous damper, the cable vibrates nearly unimpeded, and approaching an infinite damping constant, the cable again vibrates nearly unimpeded but in the span beyond the location of the attached damper; the optimum, then, must fall somewhere in between. Fujino and colleagues (Sulekh, 1990; Pacheco *et al.*, 1993) derived an approximate relationship that may be used to estimate the optimal damper design for a given cable configuration and attachment location.

Several studies (*e.g.*, Kovacs, 1982; Pacheco *et al.*, 1993; Krenk, 2000; Main and Jones, 2002a) have shown that the maximum amount of damping added to the cable with a transverse passive linear damper is approximately proportional to the distance, relative to the cable length, between the damper and the cable/deck anchorage. Similar damping levels are also achieved by nonlinear passive dampers (Main and Jones, 2002b; Krenk and Høgsberg, 2005). Further, any device rigidity reduces passive damper performance and while adding mass can increase damping (Krenk and Høgsberg, 2005), it is still likely to be on the same order as that of a linear passive damper. Modern cable-stayed bridges are using longer and longer cables, such as cables on the Tataru and Normandie Bridges which are more than 450 meters long (Endo *et al.*, 1991; Virloguex *et al.*, 1994) (a planned 1100 meter main-span bridge in Hong Kong (Russell, 1999) would require even longer stay cables). With such long cables, approaching a 5% connection point may be infeasible without significant changes to the aesthetics of the structure. Rather, a 1% to 2% location is more likely. In such a case, passive dampers may add insufficient damping to the cables. Therefore, other methods of mitigating excessive cable vibration must be explored.

Semiactive dampers, whether of the variable orifice, controllable friction, or controllable fluid varieties, have proven to be of significant interest in many applications (Housner *et al.*, 1997; Spencer and Sain, 1997) and can potentially achieve performance levels nearly the same as comparable active devices with few of the detractions. This paper investigates the efficacy of employing a semiactive damper as an alternative to a transverse passive viscous damper for reducing cable motion. It will be demonstrated via simulation that a semiactive device may provide dramatic reductions in cable response over the optimal linear viscous damper and achieve nearly the same performance as a comparable active damper.

CABLE DYNAMICS

Stay cables typically have small sag (on the order of 1% sag-to-length ratio) with high tension-to-weight ratios. With small sag, the inclination, the static deflection due to gravity, and the flexural rigidity may be neglected since they are second order effects. Consequently, the motion of the cable may be modeled by the motion of a taut string (Irvine, 1981). Consider the transverse motion of a cable with a damper attached transverse to the cable as shown in Fig. 1. For small deflection, this system has the following nondimensional partial differential equation of motion

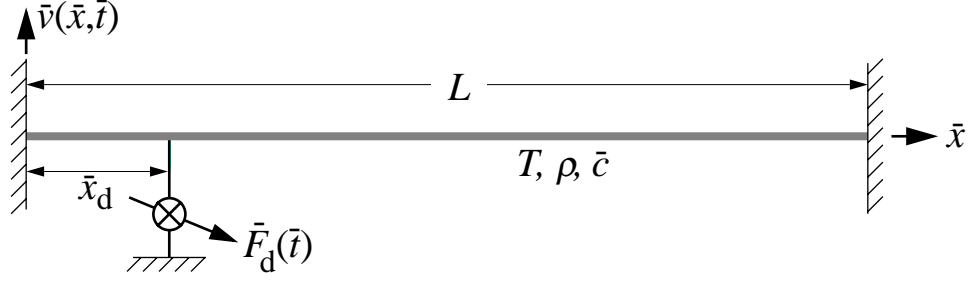


Figure 1: Cable with Attached Damper (parameters here are dimensional).

$$\ddot{v}(x, t) + c\dot{v}(x, t) - \frac{1}{\pi^2}v''(x, t) = f(x, t) + F_d(t)\delta(x - x_d), \quad 0 \leq x \leq 1 \quad (1)$$

with boundary conditions

$$v(0, t) = v(1, t) = 0 \quad \text{for all } t \quad (2)$$

where $v(x, t)$ is the transverse deflection of the cable, c is the viscous damping per unit length, $(\cdot)'$ and (\cdot) denote partial derivatives with respect to x and t , respectively, $f(x, t)$ is the distributed load on the cable, $F_d(t)$ is a transverse damper force at location $x = x_d$, and $\delta(\cdot)$ is the Dirac delta function. The nondimensional quantities are related to their dimensional counterparts, shown with overbars, according to the following relations

$$\begin{aligned} t = \omega_0 \bar{t} \quad x = \bar{x}/L \quad c = \bar{c}/\rho\omega_0 \quad v(x, t) = \bar{v}(\bar{x}, \bar{t})/L \quad \omega_0^2 = T\pi^2/\rho L^2 \\ \delta(x - x_d) = L\bar{\delta}(\bar{x} - \bar{x}_d) \quad f(x, t) = L\bar{f}(\bar{x}, \bar{t})/\pi^2 T \quad F_d(t) = \bar{F}_d(\bar{t})/\pi^2 T \end{aligned} \quad (3)$$

where L is the length of the cable, ω_0 is the fundamental natural frequency of the undamped cable, T is the cable tension, and ρ is the cable mass per unit length. (Note that, unless otherwise specified, all quantities in the remainder are nondimensional.)

The excitation $f(x, t)$ is assumed to be a stochastic process. For convenience, assume the excitation may be approximated by

$$f(x, t) = \sum_{i=1}^n \alpha_i(x)\beta_i(t) \quad (4)$$

where the $\alpha_i(x)$ are deterministic functions of position along the cable and the $\beta_i(t)$ are the components of a stationary, ergodic, zero-mean stochastic vector process.

Approximation using Series

The transverse deflection may be approximated using a finite series

$$v(x, t) = \sum_{j=1}^m q_j(t)\phi_j(x) \quad (5)$$

where the $q_j(t)$ are generalized displacements and the $\phi_j(x)$ are a set of shape functions that are continuous with piecewise continuous slope and that satisfy the geometric boundary conditions

$$\phi_j(0) = \phi_j(1) = 0 \quad (6)$$

Substituting (5) into the nondimensional equation of motion (1) results in

$$\sum_{j=1}^m [\ddot{q}_j(t)\phi_j(x) + c\dot{q}_j(t)\phi_j(x) - \frac{1}{\pi^2}q_j(t)\phi_j''(x)] = f(x, t) + F_d(t)\delta(x - x_d) + \Delta_m(x, t) \quad (7)$$

where $\Delta_m(x, t)$ is the truncation error. Using a standard Galerkin approach (Craig, 1981) (*i.e.*, assume the truncation error is orthogonal to the shape functions retained), multiplying (7) by $\phi_i(x)$ and integrating over the length of the cable gives

$$\sum_{j=1}^m [m_{ij}\ddot{q}_j(t) + c_{ij}\dot{q}_j(t) + k_{ij}q_j(t)] = f_i(t) + F_d(t)\phi_i(x_d) \quad (8)$$

where

$$\begin{aligned} m_{ij} &= \int_0^1 \phi_i(x)\phi_j(x)dx & c_{ij} &= c \int_0^1 \phi_i(x)\phi_j(x)dx \\ k_{ij} &= -\frac{1}{\pi^2} \int_0^1 \phi_i(x)\phi_j''(x)dx & f_i(t) &= \int_0^1 f(x, t)\phi_i(x)dx \end{aligned} \quad (9)$$

Integration by parts can be performed on the stiffness term k_{ij} in (9) (the shape functions $\phi_j(x)$ vanish at the integration limits) to get

$$k_{ij} = \frac{1}{\pi^2} \int_0^1 \phi_i'(x)\phi_j'(x)dx \quad (10)$$

The equation of motion can then be written in matrix form

$$\mathbf{M}\ddot{\mathbf{q}} + \mathbf{C}\dot{\mathbf{q}} + \mathbf{K}\mathbf{q} = \mathbf{f} + \boldsymbol{\phi}F_d(t) \quad (11)$$

with mass $\mathbf{M} = [m_{ij}]$, damping $\mathbf{C} = [c_{ij}]$, and stiffness $\mathbf{K} = [k_{ij}]$ matrices, generalized displacement vector $\mathbf{q} = [q_i(t)]$, externally applied load vector $\mathbf{f} = \mathbf{f}(t) = [f_1 \ f_2 \ \dots \ f_m]^T$, and damper load vector

$$\boldsymbol{\phi} = \boldsymbol{\phi}(x_d) = [\phi_1(x_d) \ \phi_2(x_d) \ \dots \ \phi_m(x_d)]^T \quad (12)$$

Solution by Sine Series Approximation

Pacheco *et al.* (1993) assumed sinusoidal shape functions, $\phi_i(x) = \sin \pi i x$, identical to the mode shapes of the cable without the damper, to compute the damping with attached viscous

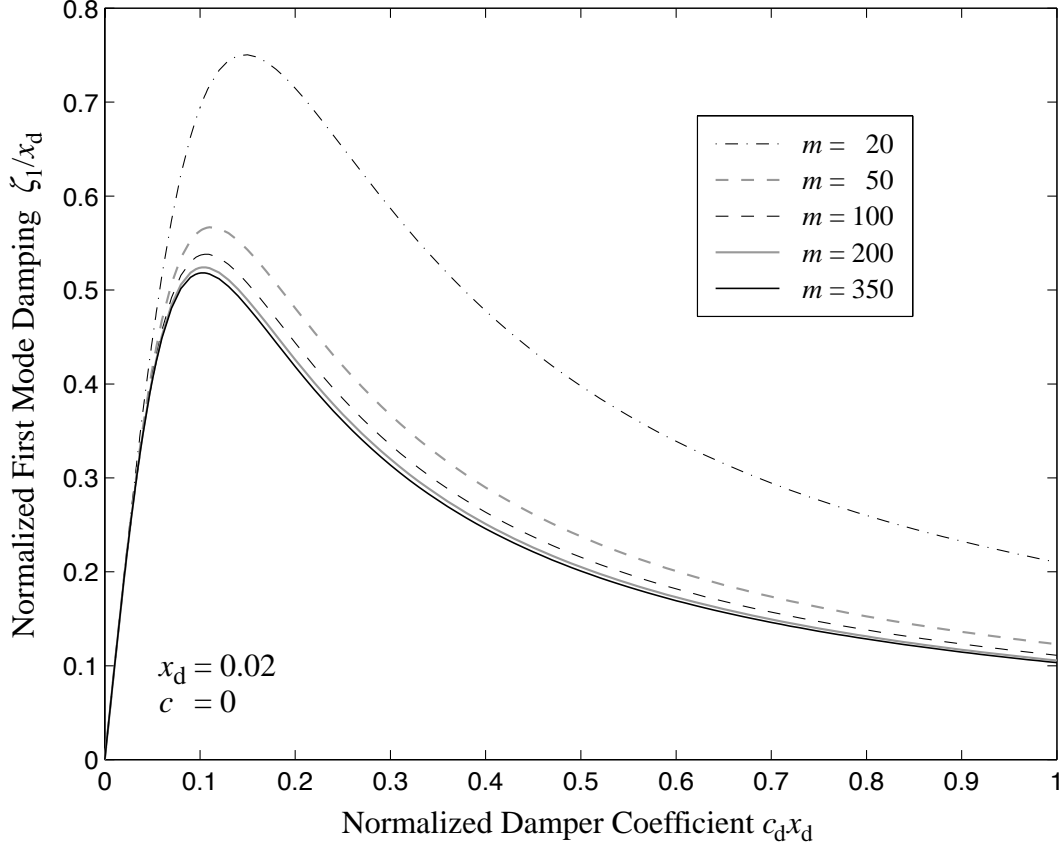


Figure 2: Modal Damping for a Range of Damper Coefficients.

dampers. Since these sinusoidal shape functions are mutually orthogonal, the mass, damping and stiffness matrices are diagonal and the system decouples into the form

$$\ddot{q}_i(t) + c\dot{q}_i(t) + i^2q_i(t) = 2f_i(t) + 2\varphi_i F_d(t), \quad i = 1, \dots, m \quad (13)$$

Using a linear viscous damper, $F_d(t) = -c_d \dot{v}(x_d, t)$, the cable/damper system may be posed in state space form as

$$\begin{Bmatrix} \dot{\mathbf{q}} \\ \ddot{\mathbf{q}} \end{Bmatrix} = \begin{bmatrix} \mathbf{0} & \mathbf{I} \\ -[i^2\delta_{ij}] & -c\mathbf{I} - 2c_d\boldsymbol{\varphi}\boldsymbol{\varphi}^T \end{bmatrix} \begin{Bmatrix} \mathbf{q} \\ \dot{\mathbf{q}} \end{Bmatrix} + \begin{bmatrix} \mathbf{0} \\ 2\mathbf{I} \end{bmatrix} \mathbf{f} \quad (14)$$

where δ_{ij} is the Kronecker delta. (Note: the c_d used here is nondimensional; the corresponding dimensional term is given by $\bar{c}_d = \rho\omega_0 Lc_d$.) A simple eigenvalue analysis of the state matrix in (14) may be used to compute the damping in the system. Figure 2 shows the normalized modal damping as a function of the damper coefficient c_d ; this particular graph was generated using the first mode with a damper location $x_d = 0.02$, but is similar for other damper locations and other modes (Pacheco *et al.*, 1993). Additionally, the inherent cable damping c was assumed here to be zero; typical values of c for real cables are sufficiently small that the graph would change insignificantly. Two important observations may be drawn from Fig. 2. First, there is a linear viscous damper that maximizes the damping in the first mode, as was observed in a number of previous studies (*e.g.*, Kovacs, 1982; Sulekh, 1990; Pacheco *et al.*, 1993). Second, as was also noted by

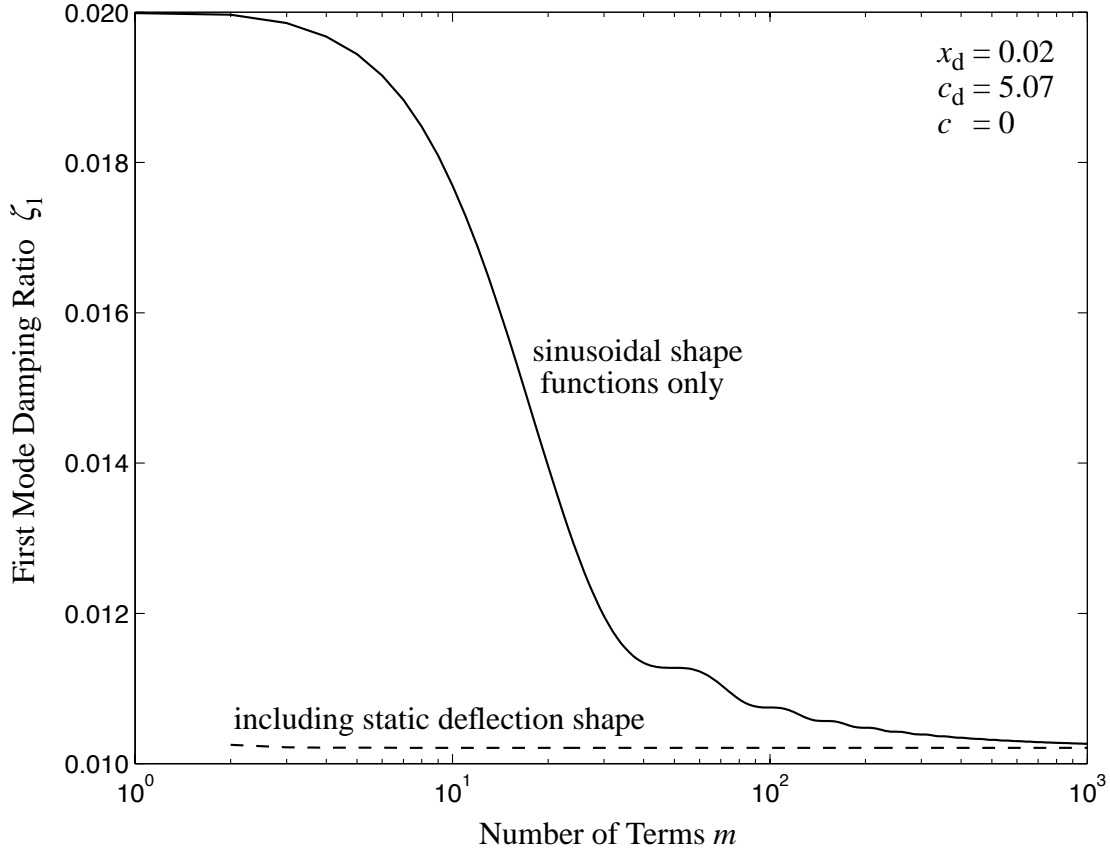


Figure 3: First Mode Damping Convergence.

Pacheco *et al.* (1993), the number of terms required to accurately compute the optimal damping is quite large. This observation may also be seen in Fig. 3, which shows the computed value of ζ_1 , the damping ratio in the first mode, as a function of the number of terms used in the series approximation for the optimal damper coefficient ($c_d = 5.07$) at location $x_d = 0.02$. The series using sinusoidal shape functions converges rather slowly, requiring hundreds of shape functions for convergence of ζ_1 .

Development of a Control-Oriented Model

Using several hundred terms in the sine series to compute the system eigenvalues, and even to simulate the system, is possible on today's computers, though it does take considerable computation effort. However, when trying to use active or semiactive control of the system, controllers for systems of such complexity are problematic in the control design, evaluation and implementation stages (*e.g.*, numerical conditioning can become poor for the matrices used in control design for large systems, the computation speed in implementing controllers is limited, *etc.*). A control-oriented model of modest order is required.

Much of the demand for using so many terms in the series is associated with the need to approximate the kink in the damped modes of the combined cable/damper system such as shown in Fig. 5c. Introducing a shape function based on the deflection due to a static force at the damper

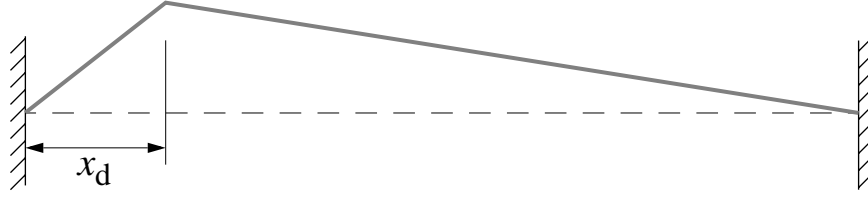


Figure 4: Static Deflection Shape Function.

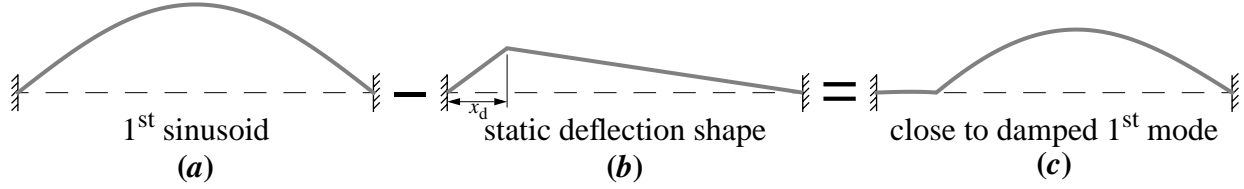


Figure 5: Simple Approximation of First Damped Eigenfunction.

location can reduce this demand. The static deflection shape function is shown in Fig. 4 and is given by

$$\phi_1(x) = \begin{cases} x/x_d, & 0 \leq x \leq x_d \\ (1-x)/(1-x_d), & x_d \leq x \leq 1 \end{cases} \quad (15)$$

Using a linear combination of the static deflection shape and the first sine term, as shown in Fig. 5, closely approximates the first damped eigenfunction of the system with a passive linear viscous damper with high damping coefficient. Consequently, including the static deflection as a shape function should allow two terms in the series to closely approximate the first mode of the combined cable/damper system and, therefore, decrease the number of terms required for comparable accuracy.

The other shape functions remain sinusoidal, $\phi_{j+1}(x) = \sin \pi j x$, and the cable deflection is approximated by

$$v(x, t) = \sum_{j=1}^m q_j(t) \phi_j(x) \quad (16)$$

Once again, a standard Galerkin approach can be taken, resulting in mass and stiffness matrices

$$[\mathbf{M}]_{ij} = \begin{cases} \frac{1}{2}\delta_{ij}, & i > 1, j > 1 \\ \frac{1}{3}, & i = 1, j = 1 \\ \frac{\sin k\pi x_d}{x_d(1-x_d)k^2\pi^2}, & \text{otherwise} \\ & \text{where } k = \max\{i, j\} - 1 \end{cases} \quad [\mathbf{K}]_{ij} = \begin{cases} \frac{1}{2}(i-1)^2\delta_{ij}, & i > 1, j > 1 \\ \frac{1}{x_d(1-x_d)\pi^2}, & i = 1, j = 1 \\ \frac{\sin k\pi x_d}{x_d(1-x_d)\pi^2}, & \text{otherwise} \\ & \text{where } k = \max\{i, j\} - 1 \end{cases} \quad (17)$$

and damping matrix $\mathbf{C} = c\mathbf{M}$. The state-space representation can be formulated as

$$\begin{Bmatrix} \dot{\mathbf{q}} \\ \ddot{\mathbf{q}} \end{Bmatrix} = \begin{bmatrix} \mathbf{0} & \mathbf{I} \\ -\mathbf{M}^{-1}\mathbf{K} & -\mathbf{M}^{-1}\mathbf{C} \end{bmatrix} \begin{Bmatrix} \mathbf{q} \\ \dot{\mathbf{q}} \end{Bmatrix} + \begin{bmatrix} \mathbf{0} \\ \mathbf{M}^{-1}\boldsymbol{\phi} \end{bmatrix} F_d(t) + \begin{bmatrix} \mathbf{0} \\ \mathbf{M}^{-1} \end{bmatrix} \mathbf{f} \quad (18)$$

or, equivalently,

$$\begin{aligned} \dot{\boldsymbol{\eta}} &= \mathbf{A} \boldsymbol{\eta} + \mathbf{B} F_d(t) + \mathbf{G} \mathbf{f} \\ \mathbf{z} &= \mathbf{C}_z \boldsymbol{\eta} + \mathbf{D}_z F_d(t) + \mathbf{H}_z \mathbf{f} \\ \mathbf{y} &= \mathbf{C}_y \boldsymbol{\eta} + \mathbf{D}_y F_d(t) + \mathbf{H}_y \mathbf{f} + \mathbf{v} \end{aligned} \quad (19)$$

where $\boldsymbol{\eta} = [\mathbf{q}^T \quad \dot{\mathbf{q}}^T]^T$ is the state vector, $\mathbf{z} = [\mathbf{q}^T \quad \dot{\mathbf{q}}^T \quad \ddot{\mathbf{q}}^T]^T$ is a vector of quantities to be regulated (includes the generalized displacements, velocities, and terms $\ddot{\mathbf{q}} = \ddot{\mathbf{q}} - \mathbf{M}^{-1}\mathbf{f}$ related to the generalized accelerations), $\mathbf{y} = [v(x_d, t) \quad \dot{v}(x_d, t)]^T + \mathbf{v}$ is a vector of noisy sensor measurements (includes the displacement and acceleration at the damper location), \mathbf{v} is a vector of stochastic sensor noise processes, and

$$\begin{aligned} \mathbf{A} &= \begin{bmatrix} \mathbf{0} & \mathbf{I} \\ -\mathbf{M}^{-1}\mathbf{K} & -\mathbf{M}^{-1}\mathbf{C} \end{bmatrix} & \mathbf{B} &= \begin{bmatrix} \mathbf{0} \\ \mathbf{M}^{-1}\boldsymbol{\phi} \end{bmatrix} & \mathbf{G} &= \begin{bmatrix} \mathbf{0} \\ \mathbf{M}^{-1} \end{bmatrix} \\ \mathbf{C}_z &= \begin{bmatrix} \mathbf{I} & \mathbf{0} \\ \mathbf{0} & \mathbf{I} \\ -\mathbf{M}^{-1}\mathbf{K} & -\mathbf{M}^{-1}\mathbf{C} \end{bmatrix} & \mathbf{D}_z &= \begin{bmatrix} \mathbf{0} \\ \mathbf{0} \\ \mathbf{M}^{-1}\boldsymbol{\phi} \end{bmatrix} & \mathbf{H}_z &= \begin{bmatrix} \mathbf{0} \\ \mathbf{0} \\ \mathbf{0} \end{bmatrix} \\ \mathbf{C}_y &= \begin{bmatrix} \boldsymbol{\phi}^T & \mathbf{0} \\ -\boldsymbol{\phi}^T\mathbf{M}^{-1}\mathbf{K} & -\boldsymbol{\phi}^T\mathbf{M}^{-1}\mathbf{C} \end{bmatrix} & \mathbf{D}_y &= \begin{bmatrix} \mathbf{0} \\ \boldsymbol{\phi}^T\mathbf{M}^{-1}\boldsymbol{\phi} \end{bmatrix} & \mathbf{H}_y &= \begin{bmatrix} \mathbf{0} \\ \boldsymbol{\phi}^T\mathbf{M}^{-1} \end{bmatrix} \end{aligned} \quad (20)$$

Assessment of Control-Oriented Cable Model

A control-oriented model of the cable should, with only a few terms, adequately describe the dynamic characteristics of the cable, including the natural frequency ω_i , damping ratio ζ_i , and eigenfunction $\tilde{\phi}_i(x)$ for each mode. To investigate the convergence rate for the two series approximations, consider the passive linear viscous damper located at $x_d = 0.02$ that maximizes the

damping in the first mode (the optimal damper coefficient for this damper location is $c_d = 5.07$). Figure 3 shows that the damping in the first mode converges *very* fast when using the static deflection shape compared to without it. In fact, the relative error in the damping estimate computed using only the static deflection shape and the first sinusoid is less than 0.001, compared to over 1000 sinusoids alone for the same accuracy. Similar trends occur for higher modes as well.

A second test of the convergence of the cable model is to examine the convergence of the damping as a function of the viscous damper coefficient. Figure 6 shows the normalized modal

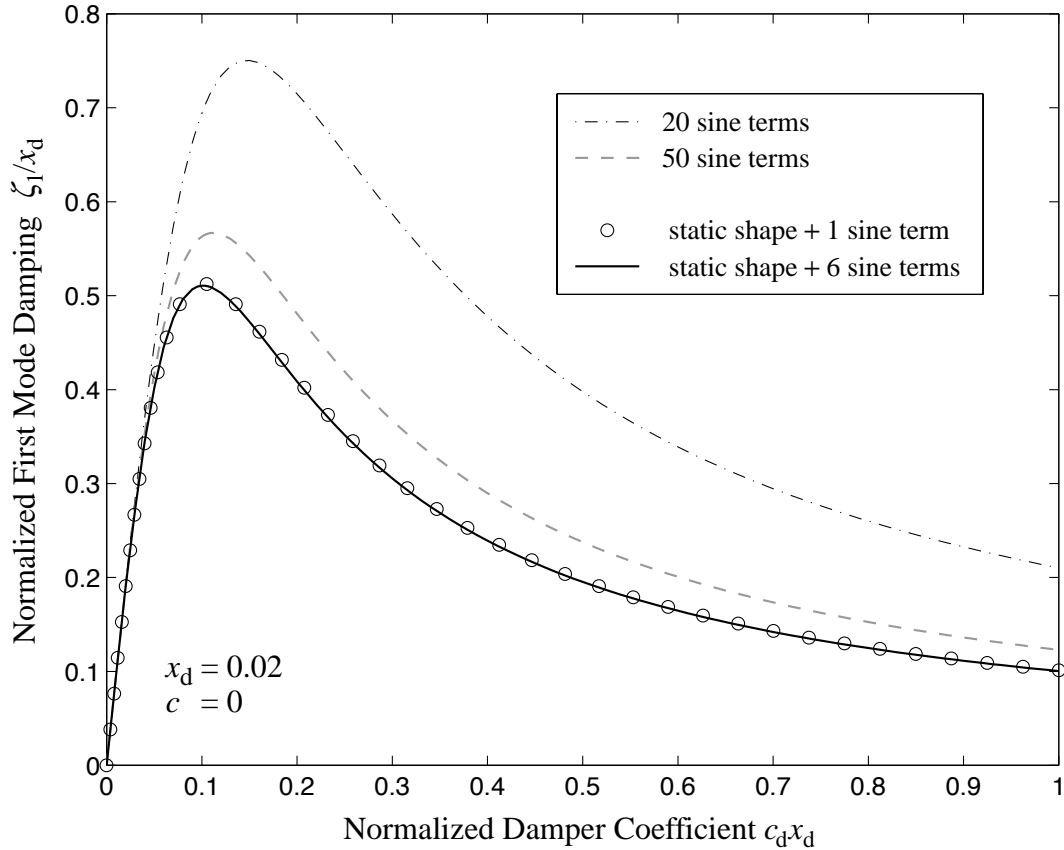


Figure 6: Modal Damping for Range of Damper Coefficients with and without Static Deflection Shape Function.

damping with and without the static deflection shape function for several numbers of terms in the series. Again, including the static deflection shape allows the same accuracy with only a few terms as would be attained with hundreds of terms in the sine-only series.

A third demonstration of the convergence properties may be seen by computing the error in the first several eigenfunctions (*i.e.*, the mode shapes of the combined system). Define the relative eigenfunction error as

$$\text{relative eigenfunction error} = \frac{\|\tilde{\phi}_i^m(x) - \tilde{\phi}_i^{499s + sd}(x)\|_2}{\|\tilde{\phi}_i^{499s + sd}(x)\|_2} \quad (21)$$

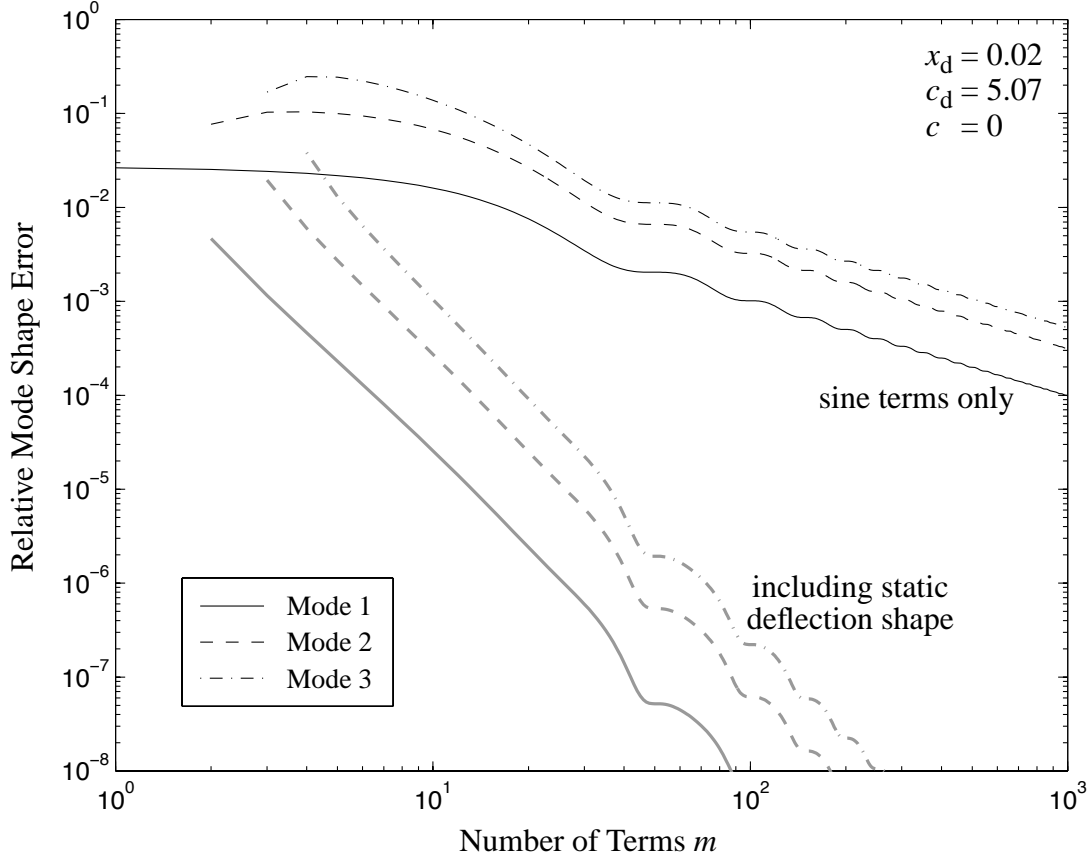


Figure 7: Normalized Error in Eigenfunctions.

where $\tilde{\phi}_i^m(x)$ is the i^{th} eigenfunction computed using m shape functions, $\tilde{\phi}_i^{499s+sd}(x)$ is the i^{th} eigenfunction when using 499 sine terms plus the static deflection shape (used here as the measure against which less accurate models are compared), and $\|\cdot\|_2$ is a standard 2-norm defined by

$$\|\cdot\|_2^2 = \int_0^1 |\cdot|^2 dx \quad (22)$$

The relative eigenfunction error (21) may be computed directly from the eigenvectors of the state matrix as described in the Appendix.

The resulting relative error as a function of m , the number of shape functions in the series, is shown in Fig. 7 for the first three modes when including and omitting the static deflection term (passive damper $c_d = 5.07$ at $x_d = 0.02$). The convergence is notably faster when including the static deflection shape; 12 sine terms plus the static deflection gives the same accuracy as 1000 sine terms alone for the first three eigenfunctions. Similar trends exist for higher modes as well.

Thus, using the static deflection shape function will provide a low-order control-oriented model with accuracy sufficient to capture the salient dynamics of the combined cable/damper system.

CONTROL OF CABLE VIBRATION

Three types of dampers are considered in this study. The damper of primary interest is a general semiactive device, one that may exert any required *dissipative* force. However, comparison with passive linear viscous dampers, similar to the oil dampers that have been installed in numerous cable-stayed bridges, is vital to demonstrate the improvements that may be possible with semiactive damping technology. Additionally, comparison with active control devices is useful as they bound the achievable performance.

Passive Viscous Damper

If the damping device is a passive linear viscous damper, then the damper force is

$$F_d(t) = -c_d \dot{v}(x_d, t) \quad (23)$$

where c_d is a nondimensional damping constant and $\dot{v}(x_d, t)$ is the nondimensional velocity at the damper location

$$\dot{v}(x_d, t) = \sum_{i=1}^m \dot{q}_i(t) \phi_i(x_d) = \boldsymbol{\phi}^T \dot{\mathbf{q}} = [\mathbf{0}^T \quad \boldsymbol{\phi}^T] \boldsymbol{\eta} \quad (24)$$

The resulting state-space equations are

$$\begin{aligned} \dot{\boldsymbol{\eta}} &= \mathbf{A}_P \boldsymbol{\eta} + \mathbf{G} \mathbf{f} \\ \mathbf{z} &= \mathbf{C}_P \boldsymbol{\eta} + \mathbf{H}_z \mathbf{f} \end{aligned} \quad (25)$$

where

$$\mathbf{A}_P = \mathbf{A} + \begin{bmatrix} \mathbf{0} & \mathbf{0} \\ \mathbf{0} & -c_d \mathbf{M}^{-1} \boldsymbol{\phi} \boldsymbol{\phi}^T \end{bmatrix} \quad \mathbf{C}_P = \mathbf{C}_z + \begin{bmatrix} \mathbf{0} & \mathbf{0} \\ \mathbf{0} & \mathbf{0} \\ \mathbf{0} & -c_d \mathbf{M}^{-1} \boldsymbol{\phi} \boldsymbol{\phi}^T \end{bmatrix} \quad (26)$$

As noted above, the modal damping may be determined for this system via a straightforward eigenvalue analysis. When the distributed viscous damping is negligible, which is typically the case for long stay cables, Figs. 2 and 6 show the damping ratio for various levels of viscous damping c_d . It may be noted that the shape of the curve this curve is similar for higher modes but with the peak at different locations; consequently, the optimal choice of c_d is different for maximizing the modal damping for different modes of the combined system.

Alternate Measures of Damper Performance

Modal damping ratios provide a useful means of determining the effectiveness of linear viscous damping strategies. However, using a semiactive damper introduces a nonlinearity into the combined system. Consequently, performance measures other than modal damping must be used for judging the efficacy of nonlinear damping strategies in comparison with linear (passive or active) dampers.

Using the root mean square (RMS) or peak response of the cable at some particular location (or several locations) is one possible measure of damper performance. However, it may be possible for one control strategy to decrease the motion significantly in some regions of a structure but allow other parts to vibrate relatively unimpeded. Thus, the primary measure of damper performance considered herein is the root mean square (RMS) cable deflection $\sigma_{\text{displacement}}$ defined by

$$\begin{aligned}\sigma_{\text{displacement}}^2(t) &= E\left[\int_0^1 v^2(x, t) dx\right] = E\left[\int_0^1 \left\{\sum_{i=1}^m q_i(t) \phi_i(x)\right\}^2 dx\right] \\ &= \sum_{i=1}^m \sum_{j=1}^m E[q_i(t) q_j(t)] \int_0^1 \phi_i(x) \phi_j(x) dx = \sum_{i=1}^m \sum_{j=1}^m m_{ij} E[q_i(t) q_j(t)] \quad (27) \\ &= E[\mathbf{q}^T(t) \mathbf{M} \mathbf{q}(t)] = E[\text{trace}\{\mathbf{M}^{1/2} \mathbf{q}(t) \mathbf{q}^T(t) \mathbf{M}^{1/2}\}] \\ &= \text{trace}\{\mathbf{M}^{1/2} E[\mathbf{q}(t) \mathbf{q}^T(t)] \mathbf{M}^{1/2}\}\end{aligned}$$

where $\mathbf{M}^{1/2}$ is a square symmetric matrix such that $\mathbf{M}^{1/2} \mathbf{M}^{1/2} = \mathbf{M}$. The corresponding RMS cable velocity may be computed from the generalized velocities

$$\sigma_{\text{velocity}}^2(t) = E[\dot{\mathbf{q}}^T(t) \mathbf{M} \dot{\mathbf{q}}(t)] = \text{trace}\{\mathbf{M}^{1/2} E[\dot{\mathbf{q}}(t) \dot{\mathbf{q}}^T(t)] \mathbf{M}^{1/2}\} \quad (28)$$

Similarly, a term related to the cable acceleration may be computed from

$$\sigma_{\text{a}}^2(t) = E[\ddot{\mathbf{q}}^T(t) \mathbf{M} \ddot{\mathbf{q}}(t)] = \text{trace}\{\mathbf{M}^{1/2} E[\ddot{\mathbf{q}}(t) \ddot{\mathbf{q}}^T(t)] \mathbf{M}^{1/2}\} \quad (29)$$

where $\ddot{\mathbf{q}} = \ddot{\mathbf{q}} - \mathbf{M}^{-1} \mathbf{f}$ (*i.e.*, the generalized acceleration minus the effect of the external load). Of course, if the focus is on the stationary response — which is the case herein — then all three of these performance measures are constant and not functions of time.

For the linear systems (passive linear viscous dampers and active dampers), these quantities may be computed by solving a Lyapunov equation. For example, if the excitation vector \mathbf{f} is a zero-mean Gaussian white noise vector process with $E[\mathbf{f}(t) \mathbf{f}^T(t + \tau)] = 2\pi \mathbf{S}_0 \delta(\tau)$ where \mathbf{S}_0 is the spectral density matrix, and the damper is a passive linear viscous damper, $\sigma_{\text{displacement}}$ may be computed from (27) where

$$E[\mathbf{q} \mathbf{q}^T] = E[[\mathbf{I} \ \mathbf{0}] \boldsymbol{\eta} \boldsymbol{\eta}^T [\mathbf{I} \ \mathbf{0}]^T] = [\mathbf{I} \ \mathbf{0}] \boldsymbol{\Sigma} [\mathbf{I} \ \mathbf{0}]^T \quad (30)$$

and where $\boldsymbol{\Sigma} = E[\boldsymbol{\eta} \boldsymbol{\eta}^T]$ is the solution of the Lyapunov equation

$$\mathbf{A}_p \boldsymbol{\Sigma} + \boldsymbol{\Sigma} \mathbf{A}_p^T + \mathbf{G} 2\pi \mathbf{S}_0 \mathbf{G}^T = \mathbf{0} \quad (31)$$

Active Damper

The optimal passive viscous damper provides one benchmark against which to judge semi-active dampers. The other end of the spectrum of control possibilities is an ideal active damper, which may exert any desired force. The performance of the actively controlled systems give a performance target for semiactive control.

Four LQR (linear quadratic regulator) control designs are considered in this study. These state feedback controllers use force proportional to the state of the system, $F_d^{\text{active}}(t) = -\mathbf{L}_k \boldsymbol{\eta}$,

where \mathbf{L}_k is the feedback gain that minimizes one of four cost functions. The first controller, using cost J_1 , weights the cable displacement $\sigma_{\text{displacement}}^2$, the second the velocity $\sigma_{\text{velocity}}^2$, the third a combination of displacement and velocity $\frac{1}{2}\sigma_{\text{displacement}}^2 + \frac{1}{2}\sigma_{\text{velocity}}^2$, and the fourth a term σ_a^2 related to the acceleration. These cost functions can be written in general form

$$J_k = \lim_{T \rightarrow \infty} E \left[\frac{1}{T} \int_0^T (\mathbf{z}^T \mathbf{Q}_k \mathbf{z} + R F_d^2) dt \right], \quad k = 1, 2, 3, 4 \quad (32)$$

where

$$\mathbf{Q}_1 = \begin{bmatrix} \mathbf{M} & \mathbf{0} & \mathbf{0} \\ \mathbf{0} & \mathbf{0} & \mathbf{0} \\ \mathbf{0} & \mathbf{0} & \mathbf{0} \end{bmatrix} \quad \mathbf{Q}_2 = \begin{bmatrix} \mathbf{0} & \mathbf{0} & \mathbf{0} \\ \mathbf{0} & \mathbf{M} & \mathbf{0} \\ \mathbf{0} & \mathbf{0} & \mathbf{0} \end{bmatrix} \quad \mathbf{Q}_3 = \begin{bmatrix} \frac{1}{2}\mathbf{M} & \mathbf{0} & \mathbf{0} \\ \mathbf{0} & \frac{1}{2}\mathbf{M} & \mathbf{0} \\ \mathbf{0} & \mathbf{0} & \mathbf{0} \end{bmatrix} \quad \mathbf{Q}_4 = \begin{bmatrix} \mathbf{0} & \mathbf{0} & \mathbf{0} \\ \mathbf{0} & \mathbf{0} & \mathbf{0} \\ \mathbf{0} & \mathbf{0} & \mathbf{M} \end{bmatrix} \quad (33)$$

The feedback gain that minimizes the cost (32) is

$$\mathbf{L}_k = (R + \mathbf{D}_z^T \mathbf{Q}_k \mathbf{D}_z)^{-1} (\mathbf{B}^T \mathbf{P}_k + \mathbf{D}_z^T \mathbf{Q}_k \mathbf{C}_z) \quad (34)$$

where \mathbf{P}_k satisfies the algebraic Riccati equation

$$\mathbf{A}^T \mathbf{P}_k + \mathbf{P}_k \mathbf{A} - (\mathbf{P}_k \mathbf{B} + \mathbf{C}_z^T \mathbf{Q}_k \mathbf{D}_z) (R + \mathbf{D}_z^T \mathbf{Q}_k \mathbf{D}_z)^{-1} (\mathbf{B}^T \mathbf{P}_k + \mathbf{D}_z^T \mathbf{Q}_k \mathbf{C}_z) = -\mathbf{C}_z^T \mathbf{Q}_k \mathbf{C}_z \quad (35)$$

Varying the control weight R will then give four families of state feedback controllers. Note that because of the certainty equivalence principle (*e.g.*, Stengel, 1986), the zero-mean external excitation vector \mathbf{f} drops out of the state feedback control design.

Of course, it is unreasonable to assume that one has perfect full state information for a cable system. Consequently, some of the designs in this study use a Kalman filter to estimate the states of the system based on (noisy) sensor measurements of displacement and acceleration at the damper location. (These two measurements are likely to be the easiest to use in a full-scale implementation as they could be packaged as a part of the damper system.) The resulting estimator is dynamic with order equal to that of the cable state space model, and is given by

$$\dot{\hat{\boldsymbol{\eta}}} = \mathbf{A}_{\text{KF}} \hat{\boldsymbol{\eta}} + \mathbf{B}_{\text{KF}} \mathbf{y} + \mathbf{G}_{\text{KF}} F_d(t) \quad (36)$$

where $\hat{\boldsymbol{\eta}}$ is an estimate of the states $\boldsymbol{\eta}$, and

$$\mathbf{A}_{\text{KF}} = \mathbf{A} - \mathbf{L}_{\text{KF}} \mathbf{C}_y, \quad \mathbf{B}_{\text{KF}} = \mathbf{L}_{\text{KF}}, \quad \mathbf{G}_{\text{KF}} = \mathbf{B} - \mathbf{L}_{\text{KF}} \mathbf{D}_y \quad (37)$$

where $\mathbf{L}_{\text{KF}} = (\tilde{\mathbf{P}} \mathbf{C}_y^T + \mathbf{G} \mathbf{Q}_{\text{KF}} \mathbf{H}^T) (\mathbf{R}_{\text{KF}} + \mathbf{H} \mathbf{Q}_{\text{KF}} \mathbf{H}^T)^{-1}$ is the estimator gain and $\tilde{\mathbf{P}}$ is computed from the Riccati equation

$$\mathbf{A} \tilde{\mathbf{P}} + \tilde{\mathbf{P}} \mathbf{A}^T - (\tilde{\mathbf{P}} \mathbf{C}_y^T + \mathbf{G} \mathbf{Q}_{\text{KF}} \mathbf{H}^T) (\mathbf{R}_{\text{KF}} + \mathbf{H} \mathbf{Q}_{\text{KF}} \mathbf{H}^T)^{-1} (\mathbf{C}_y \tilde{\mathbf{P}} + \mathbf{H}_y \mathbf{Q}_{\text{KF}} \mathbf{G}^T) = -\mathbf{G} \mathbf{Q}_{\text{KF}} \mathbf{G}^T \quad (38)$$

where \mathbf{Q}_{KF} is the magnitude of the excitation spectral density $\mathbf{S}_{\text{ff}}(\omega)$, \mathbf{R}_{KF} the magnitude of noise spectral density $\mathbf{S}_{\text{vv}}(\omega)$, $E[\mathbf{f}] = \mathbf{0}$, $E[\mathbf{v}] = \mathbf{0}$, and excitation \mathbf{f} and sensor noise \mathbf{v} are uncorrelated. The force, then, is given by $F_d^{\text{active}}(t) = -\mathbf{L}_k \hat{\boldsymbol{\eta}}$.

Semiactive Damper

Unlike an active device, a semiactive damper, such as a variable-orifice viscous damper, a controllable friction damper, or a controllable fluid damper (Spencer and Sain, 1997; Fujino *et al.*, 1996; Housner *et al.*, 1997), can ideally only exert *dissipative* forces. Herein, a generic semiactive device model is assumed that is purely dissipative. Essentially, this requirement dictates that the force exerted by the damper and the velocity across the damper must be of opposite sign; *i.e.*, $F_d(t)\dot{v}(x_d, t)$ must be less than zero. Figure 8 shows this constraint graphically. (In many physical semiactive devices, there are also maximum force levels; this limit is neglected here.) This generic semiactive device model gives a first approximation of the performance potential possible with smart dampers.

In previous studies of the control of semiactive dampers (*e.g.*, Dyke *et al.*, 1996a,b; Johnson *et al.*, 1999a,b), a clipped optimal strategy, employing a two-stage control design, has performed well. The control algorithm considered here falls into this category. The primary controller is one of the same LQR or LQG control designs used for the active damper. The secondary controller, which accounts for the nonlinear nature of the semiactive device, may be given by

$$F_d(t) = \begin{cases} \alpha(\dot{v}(x_d, t))F_d^{\text{active}}(t), & F_d^{\text{active}}(t)\dot{v}(x_d, t) < 0 \\ 0, & \text{otherwise} \end{cases} \quad (39)$$

Primarily, this secondary controller ensures that the control system does not command non-dissipative damper forces. Of course, in a physical device (as opposed to simulation), this restriction is enforced by the nature of the device. (However, one would still need a secondary controller for the physical device since most semiactive devices are not linear in the relationship between command input and force exerted. Herein, it is assumed that as long as the force is dissipative, it can be commanded directly.)

The second purpose of this secondary controller is to modulate the force, via the function $\alpha(\cdot)$, when the velocity at the damper location is near zero; this is motivated by both physical and numerical reasons. In simulations with no modulation function, the following scenario often occurs: in one time step, the velocity has changed sign making the desired damper force dissipative, so the damper force is turned on; during the following time step, the large damper force drives the velocity back across zero but with the damper force still on and some displacement occurs so energy is incorrectly dissipated; the damper force is subsequently turned back off, which will make the velocity change sign again in the third time step. This cycle tends to repeat itself, resulting in many narrow but tall dissipation loops that cannot be repeated in a real semiactive device. Essentially, the damper is trying to lock up and make the cable velocity exactly zero at the damper location. This numerical dissipation can be reduced only by using extremely small time steps (on the order of 10^{-8} natural periods), which renders response simulation computationally intractable. Further, physical semiactive damping devices, such as MR dampers, cannot produce large damping forces for near-zero velocities (Spencer *et al.*, 1997; Yang *et al.*, 2002). Thus, in this study, the modulation function $\alpha(\dot{v}_d) = \tanh \mu \dot{v}_d$ is used. Large μ causes $\alpha(\cdot)$ to

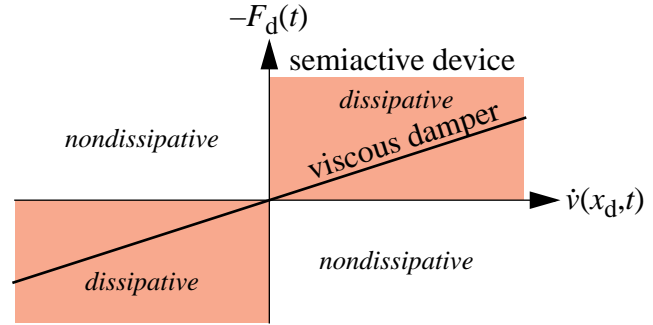


Figure 8: Semiactive Damper Dissipative Forces.

approach the $\text{sign}(\cdot)$ function, modulating only when the velocity is very small, and requiring an extremely small integration time step again. In contrast, small μ accommodates larger integration time step but can reduce the control effectiveness since it modulates the forces even at larger velocities. An extensive parameter study found that $\mu = 10$ is an acceptable trade off of control strategy performance and simulation tractability.

NUMERICAL RESULTS

A series of numerical studies were conducted to compare and contrast semiactive damper performance with that of optimal passive linear viscous dampers and linear active dampers. The inherent distributed viscous damping c was chosen to be nearly negligible: $c = 0.0001$ (which, in the absence of any other damping device, gives a damping ratio of 0.005% in the first mode). Using 20 shape functions (19 sine terms plus the static deflection term) gives less than 0.01% error in the first three combined system eigenfunctions (compared to 499 sine terms plus the static deflection term), and gave RMS response nearly identical (less than one percent error) to using more terms; consequently, all results shown below use these 20 shape functions. A range of damper locations was studied; the results discussed here are primarily for $x_d = 0.02$ but similar behavior may be observed for other small x_d .

The phenomena that cause rain-wind induced vibration, including the aerodynamic forces, motion of water rivulets, the nonlinear coupling with the cable motion, and so forth, are not well understood (Main and Jones, 1999); consequently, there are no well established models of this behavior (Scanlon, 1999). However, it has been observed that the response tends to be dominated by the first few modes. Here, the excitation is assumed to be a subset of the series in (4) using just one term

$$f(x, t) = W(t) \sin \pi x \quad (40)$$

where $W(t)$ is a zero-mean Gaussian white noise process with $E[W(t)W(t+\tau)] = \delta(\tau)$. In the absence of a damper, this excitation would result in first-mode response. The resulting generalized force vector simplifies to

$$\mathbf{f}(t) = \begin{bmatrix} \frac{\sin \pi x_d}{x_d(1-x_d)\pi^2} & \frac{1}{2} & 0 & 0 & \dots & 0 \end{bmatrix}^T W(t) \quad (41)$$

The results for the active and passive strategies are computed exactly (eigenvalue analysis for modal parameters and Lyapunov solutions for stationary response). Computing the statistics of the response for the semiactive system requires simulation due to the nonlinear nature of semiactive dampers. The RMS responses with a semiactive damper are determined from simulation time histories (generated using SIMULINK[®]) of duration 1600 to 4000 periods of the fundamental mode of the cable alone (systems with less damping require longer time histories for accurate estimation of the RMS response). The sensor noise vector \mathbf{v} is taken to be a zero-mean Gaussian white noise vector process with diagonal spectral density magnitude matrix. The magnitudes are chosen such that using band-limited white noise (nondimensional sampling time of 0.01) in the simulation (for sensor noise and excitation) gives a certain level of RMS error in each of the two sensor signals. Two different noise levels are studied here: 1% RMS sensor noise, typical of what

one might expect in practice, and 10% RMS sensor noise, included to better understand the sensitivity of the semiactive damper results to sensor noise.

Damping Ratio for Linear Control Strategies

The damping ratio in the first several modes was computed for the linear strategies, that is, for passive linear viscous dampers and for active dampers with the four state feedback control laws. Varying the damper coefficient for the passive designs and the control weight R for the active designs results in five families (one passive, four active) of combined cable/damper systems.

The effect on the first mode damping ratio is of particular interest since it may be compared to previous results using a linear viscous damper. Figure 9 shows the natural frequency and the damping ratio of the first mode of the system for the active damper with state feedback and for the passive viscous damper. (The horizontal c_d axis is scaled such that a passive system with a particular damper coefficient c_d and an active system with the corresponding control weight R use the same RMS damper force.) The peak damping ratio using a passive viscous damper is about 1%, whereas the active control may achieve 35% or higher damping ratios. The acceleration-weighting control design shows a marked decrease in the first modal frequency compared to the cable

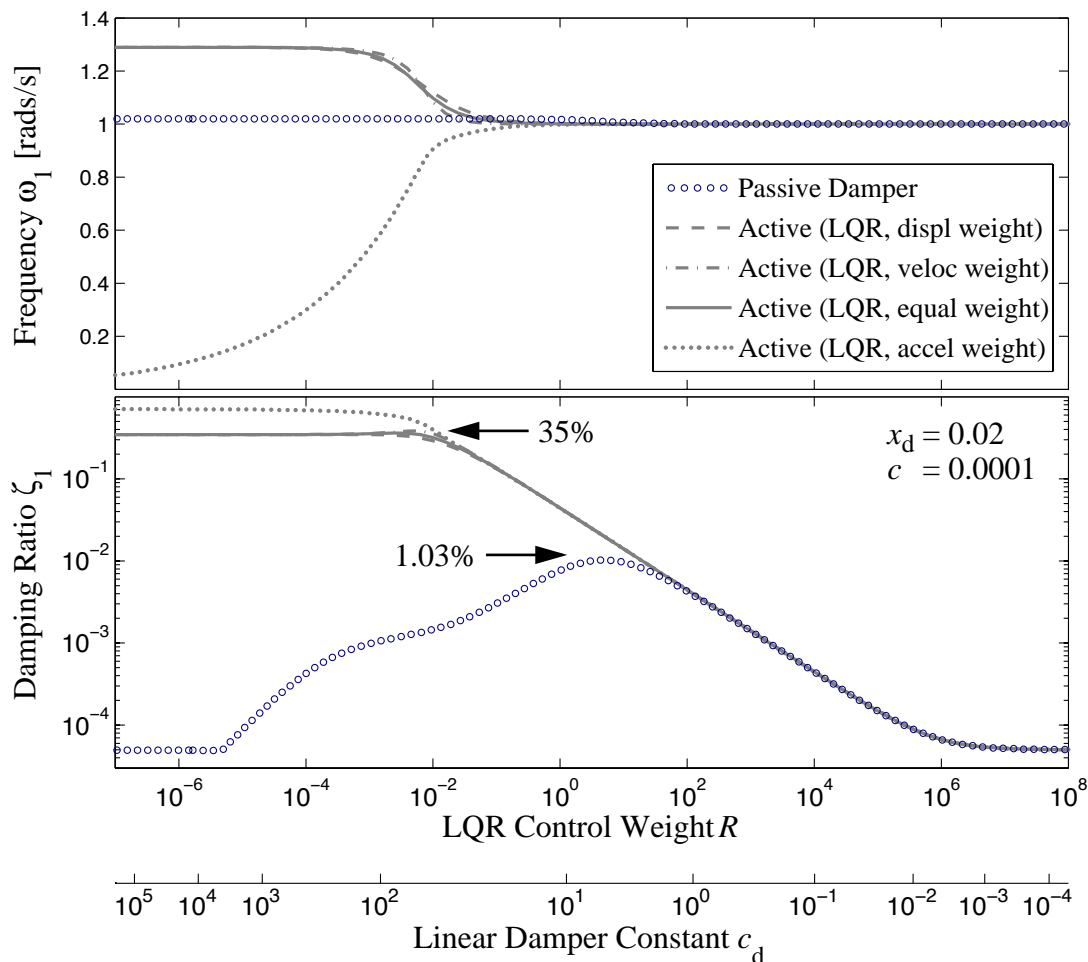


Figure 9: Natural Frequency and Damping Ratio in the First Mode for the Linear Designs.

alone. While this is not surprising, it suggests that this controller may be adding negative stiffness, which cannot be achieved with a purely dissipative semiactive device. Furthermore, negative stiffness should tend to increase displacements. Consequently, as will be shown in the next section, the acceleration-weighting control design performs poorly in simulations of the semiactive system.

RMS Cable Response

Figure 10 shows the RMS cable displacement for the passive linear viscous dampers, the active dampers with four LQR control strategies, and semiactive dampers with four clipped LQR control strategies. (As before, the passive linear viscous damper results are plotted so as to line up with that of active dampers of approximately the same RMS force.) The best viscous damper is able to achieve a significant response decrease compared to the case with no damping device. The active damper is able to further decrease that by 76.1% using the displacement weighted LQR control strategy. The clipped optimal semiactive damper with the same primary control strategy is able to do nearly as well, with 62.8% decreased RMS deflection over the optimal viscous damper. Similar trends occur for the RMS cable velocity in Fig. 11.

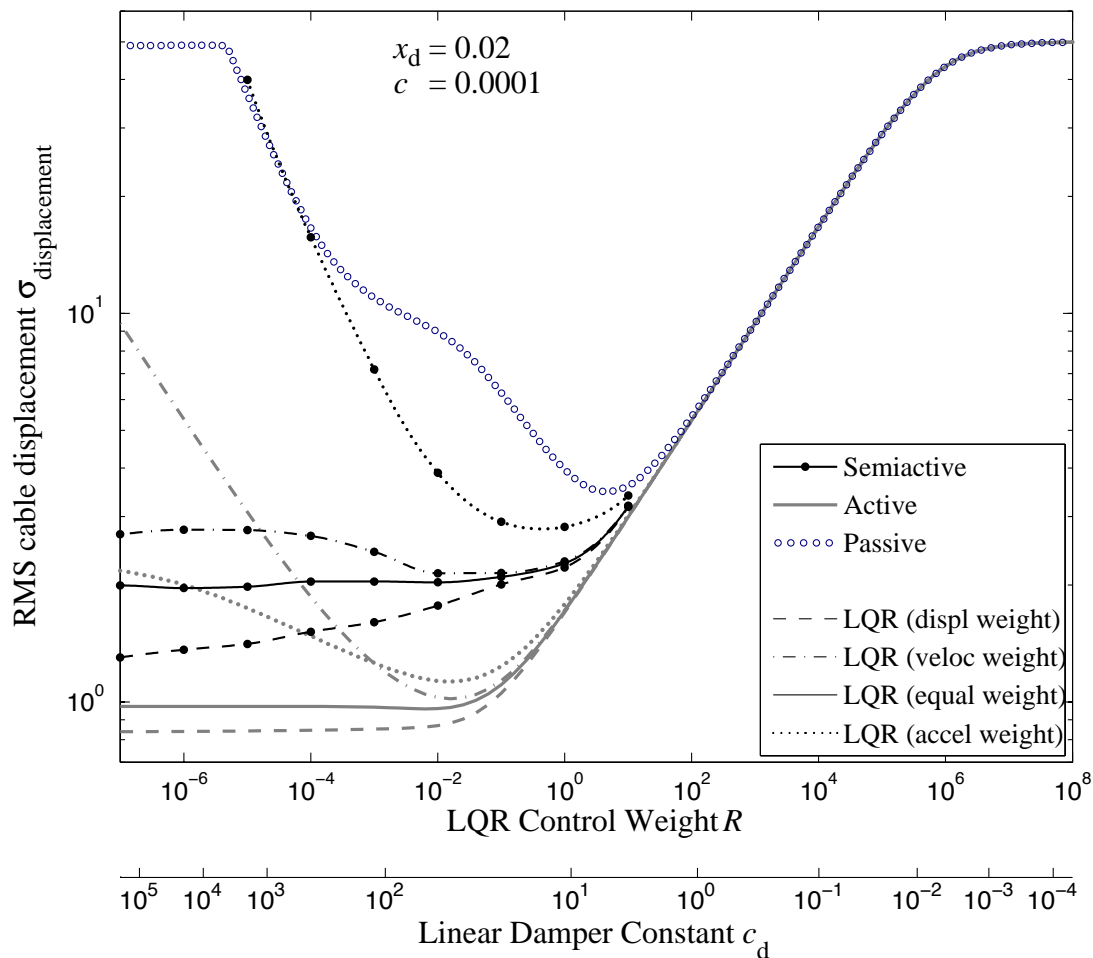


Figure 10: RMS Displacement for Semiactive, Passive Viscous, and Active Dampers.

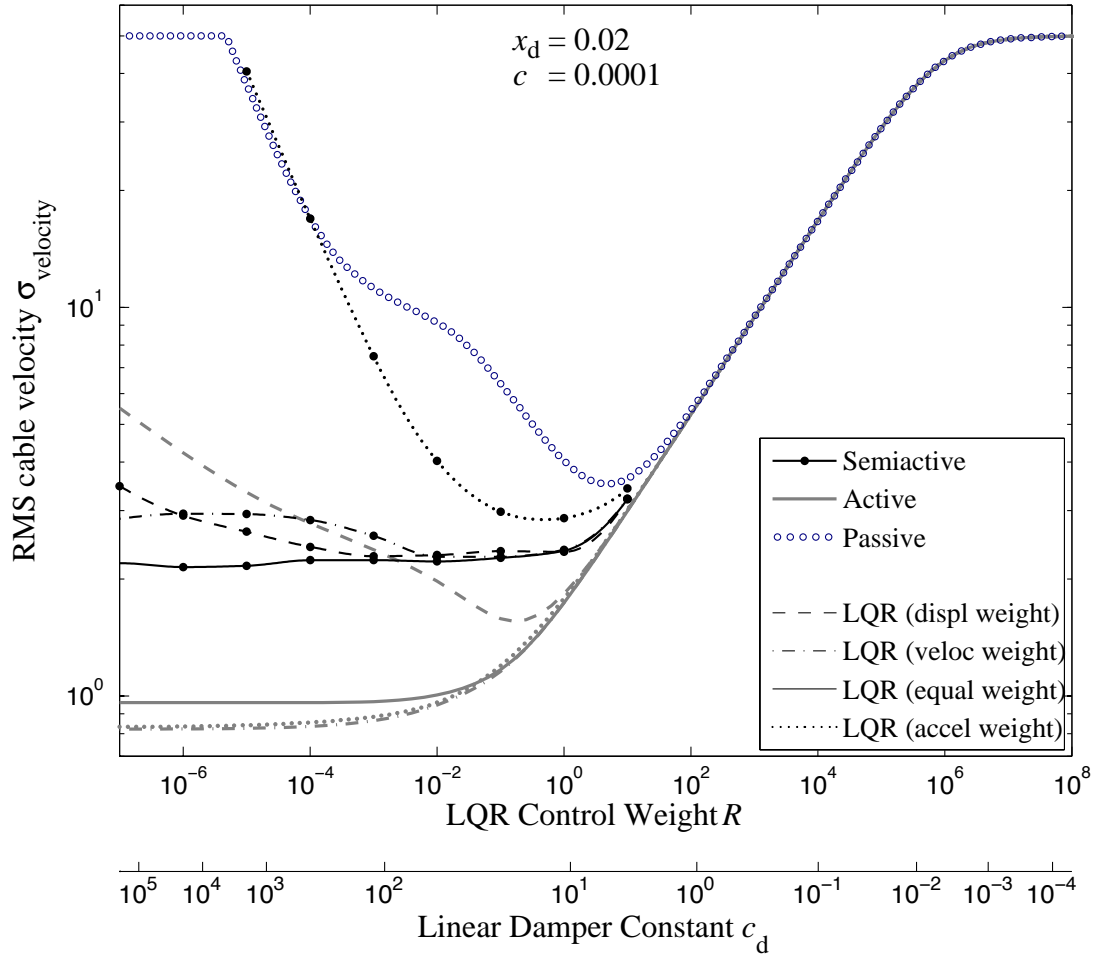


Figure 11: RMS Velocity for Semiactive, Passive Viscous, and Active Dampers.

Weighting the cable velocity, as expected, decreases cable velocity relative to the displacement-weighted control but also increases cable displacements. Weighting displacement and velocity equally gives a nice balance, but underperforms the displacement-weighted controller (though the latter uses larger damper forces). As expected, the semiactive damper with acceleration weighting performs poorly, mostly due to the primary controller commanding predominantly non-dissipative forces.

The root mean square forces exerted by the various dampers are shown in Fig. 12. The force levels are similar between the various types of dampers. The control weight R that gives minimum RMS displacement and velocity produces forces that are several times larger than the optimal passive damper (see also Table 1).

Comparison of State and Output Feedback

State feedback would require knowledge of the displacement and velocity at all points along the length of the cable. This is, of course, infeasible, so it is necessary to add a Kalman filter to estimate the states of the system based on sensor measurements. The sensors used here are the displacement and acceleration of the cable at the damper location. The responses of the cable/

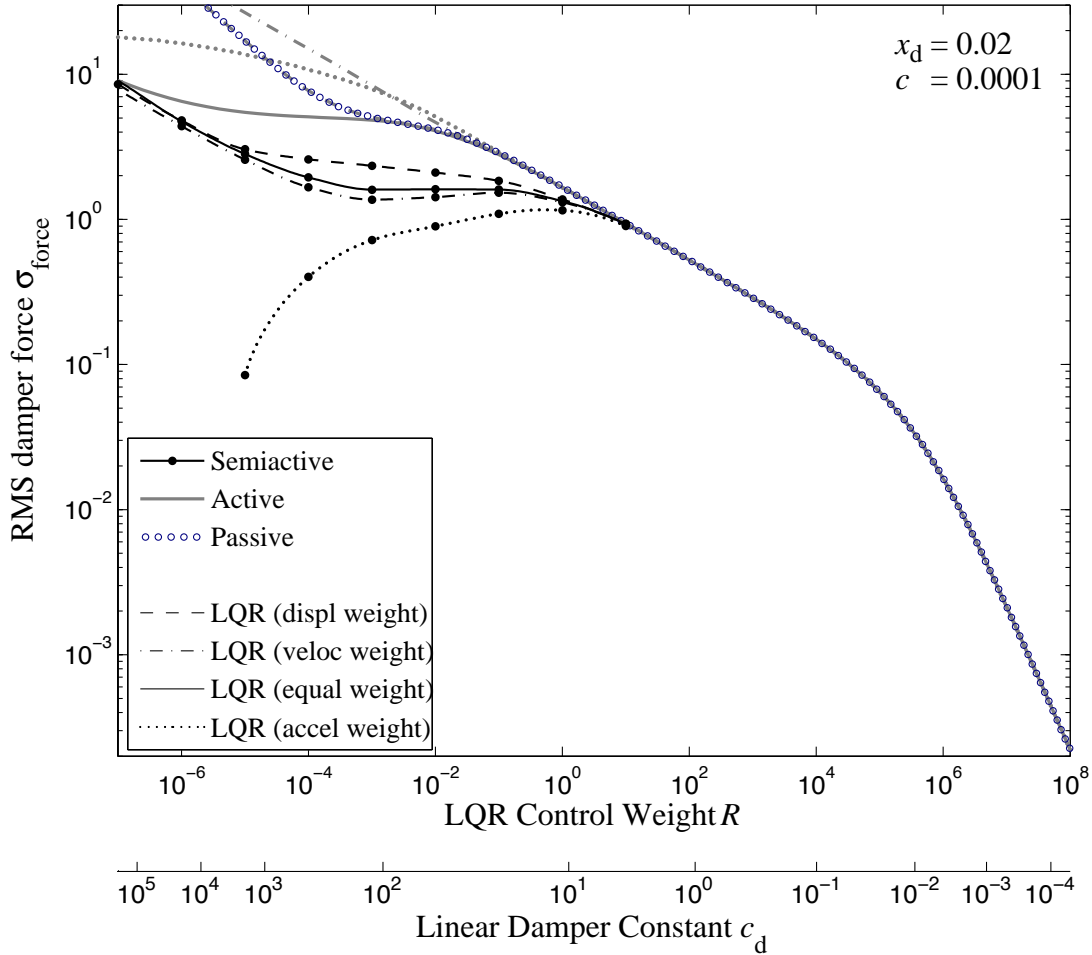


Figure 12: RMS Damper Force for Semiactive, Passive Viscous, and Active Dampers.

damper system with two values of the noise magnitude were computed, with the noise RMS being 1% of the signal RMS, and 10% of the signal RMS.

Using the displacement-weighted control (cost J_1 in the previous section) of a semiactive damper, the RMS response using state feedback (LQR) and output feedback (LQG) with both noise magnitudes was computed for a range of damper locations. At each damper location, the control weight R was chosen so as to minimize RMS cable displacement. Figure 13 shows that using output feedback control achieves nearly the same responses as the state feedback controller.

Performance of Damping Strategies over a Range of Damper Locations

The achievable performance of semiactive dampers, in comparison with active and passive devices, may be seen in Fig. 14 and in Table 1. The active and semiactive strategies here both use the displacement-weighting controller with output feedback and 1% sensor noise, and the passive damper is the linear viscous damper giving minimum response for the excitation given above in (40). At each damper location, the displacement-weighted LQG controller that best reduced the RMS displacement is used. (Due to the computational intensity required for finding the control weight R that results in the best semiactive damper performance for a particular damper location,

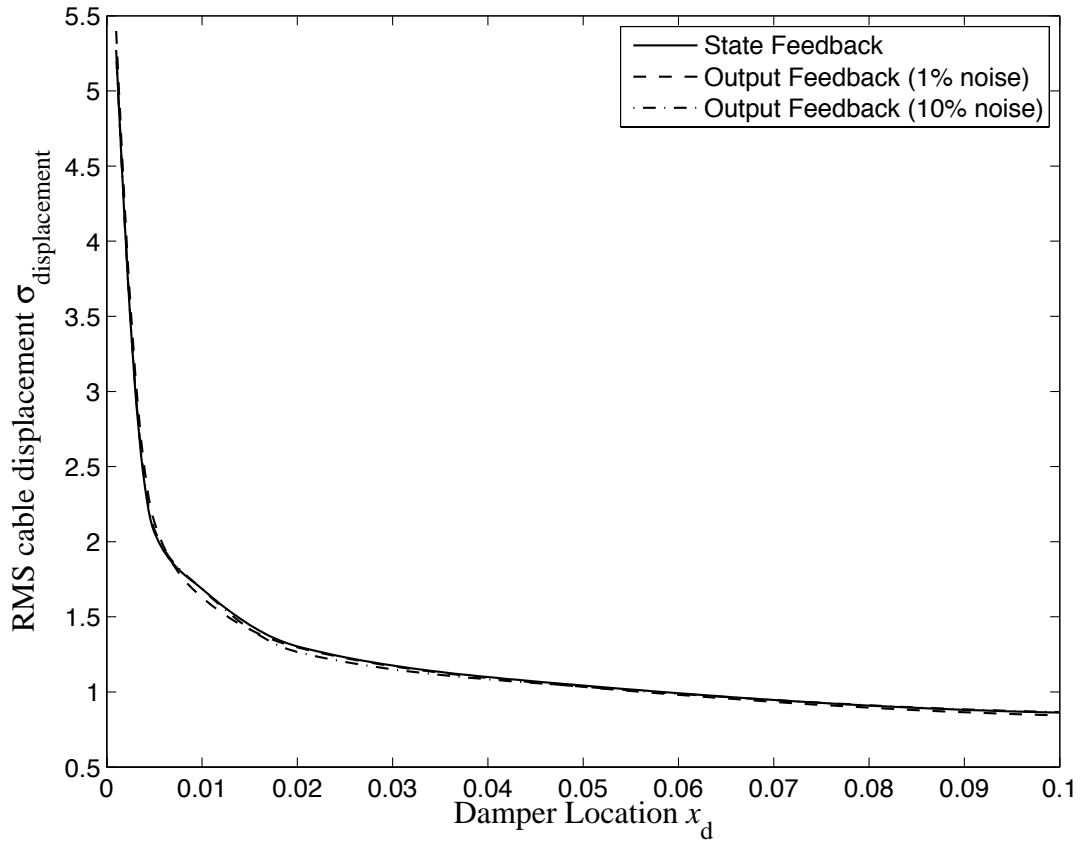


Figure 13: Comparison of State Feedback (LQR) and Output Feedback (LQG) Control (Displacement-Weighted) of a Semiactive Damper for Various Damper Locations.

a limited number of values of R were used; consequently, the true optimal semiactive performance may be slightly better (*i.e.*, lower response) than reported here.) For damper locations distant from the cable anchorage, around $x_d = 0.10$, the response reduction using a semiactive damper rather than a passive damper is good, about 43% reduction compared to the optimal passive linear viscous damper. This reduction is more significant for damper locations closer to the end of the cable: 52% reduction at $x_d = 0.05$, 63% reduction at $x_d = 0.02$, and 67% reduction at $x_d = 0.01$.

This improvement does come at the expense of larger damper forces, as may be seen in Table 1. However, the force levels are still reasonable and well within the capabilities of today's semiactive devices. For example, consider the rain-wind induced cable vibration that was observed on the Aratsu bridge, prior to the installation of passive dampers, with 60 cm peak-to-peak deflections (Yoshimura *et al.*, 1989). A semiactive damper at $x_d = 0.02$ used to reduce this motion by about 87% relative to a typical uncontrolled cable would have a peak damper forces on the order of 19 kN (4.2 kips), which is quite feasible with modern semiactive devices; this semiactive response is about 58% reduced compared to the ideal passive damper which would use peak forces around 8 kN (see the Appendix). Additionally, it is important to recall that the passive linear viscous damper results reported in Fig. 14 are the *optimal* — no better RMS performance may be achieved using such a device (for the excitation considered herein). If the semiactive

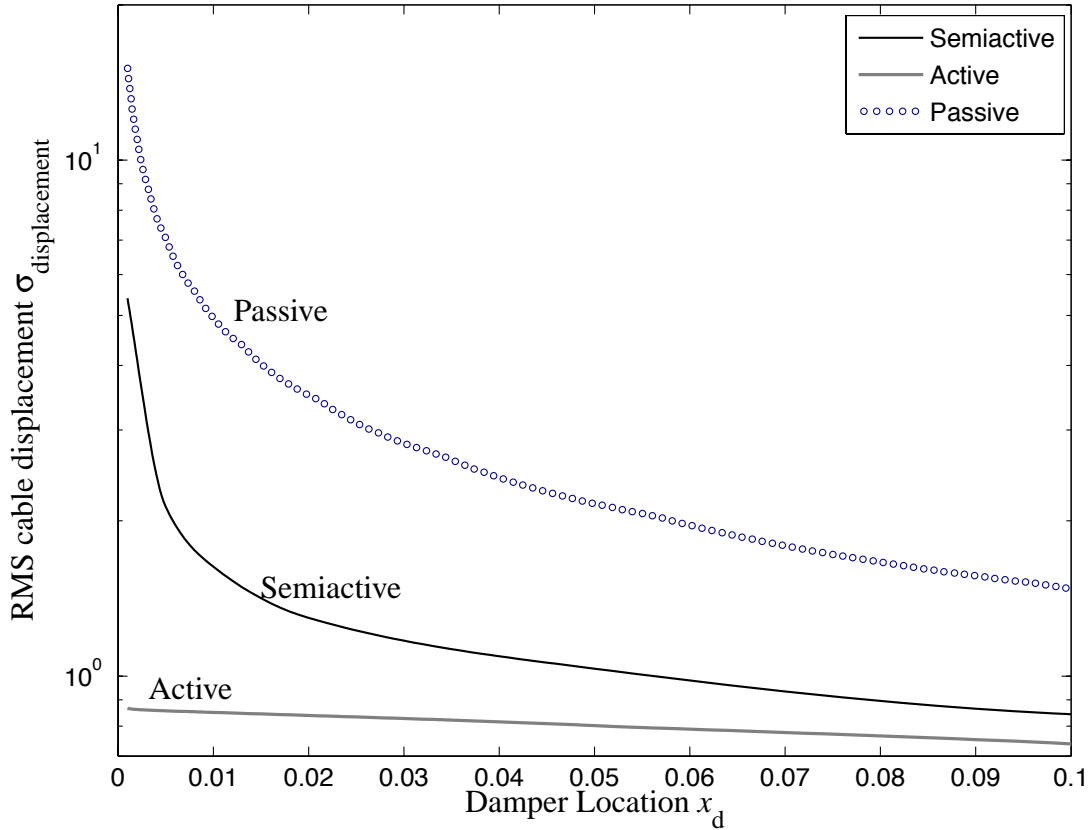


Figure 14: Comparison of Passive, Active, and Semiactive Damping Strategies for Various Damper Locations (active and semiactive use displacement-weighted, output feedback LQG controllers, and 1% sensor noise).

Table 1: Optimal Performance Values for Different Control Schemes^a

Damper Location x_d	Type of Damping Strategy	Parameter (Active/Semi. R , Passive c_d)	RMS Responses			Viscous Damping ζ_1 [%]
			Displ.	Velocity	Force	
0.01	Passive	$c_d = 10.000$	4.939	4.964	1.573	0.510
	Active	$R = 3.981 \times 10^{-7}$	0.851	4.779	58.404	34.638
	Semiactive	$R = 1.000 \times 10^{-7}$	1.630	4.942	16.029	n/a
0.02	Passive	$c_d = 6.310$	3.504	3.548	1.253	1.001
	Active	$R = 1.000 \times 10^{-7}$	0.839	5.504	101.253	34.625
	Semiactive	$R = 1.000 \times 10^{-7}$	1.297	3.386	8.414	n/a
0.05	Passive	$c_d = 2.512$	2.159	2.228	0.792	2.584
	Active	$R = 1.000 \times 10^{-7}$	0.802	5.628	99.082	34.547
	Semiactive	$R = 1.000 \times 10^{-4}$	1.034	2.416	1.736	n/a

^a Responses of active and semiactive strategies are for output feedback (LQG) control with the displacement-weighting and 1% RMS sensor noise.

force levels are too large to accommodate, there is still much room for using a less aggressive control strategy that would still improve significantly over the passive damper for small x_d . For example, with a damper location $x_d = 0.02$, the displacement-weighted, output feedback, semi-active damping strategy that gave the minimum RMS displacement response used a control weight $R = 10^{-7}$, and achieved a 63% decrease in RMS displacement compared to the optimal passive damper with RMS force 6.7 times that of the passive device. By using a slightly less aggressive control design, with a control weight $R = 10^{-4}$, the RMS response is still 57% lower than the optimal passive damper but with a force only 2.5 times that of the passive device; with $R = 10^{-2}$, the RMS displacement is 50% smaller than that with a passive viscous damper but only 1.7 times the force.

Table 1 also shows the first-mode viscous damping ratio for the passive and active systems computed from the eigenvalues of the closed-loop system. Since the semiactive damper is nonlinear, no viscous damping ratio may be computed. However, since the optimal semiactive damper provides RMS response reduction similar to that of the fully active system, it may be inferred that an “equivalent” damping ratio on the order of 8% is achievable with a semiactive device.

CONCLUSIONS

The potential of using semiactive dampers to control stay cable vibration has been demonstrated through an analysis of RMS responses and comparison with both passive linear viscous dampers and active dampers with several control designs. The limitations of the response reductions with a passive damper were reviewed. A control-oriented model using an assumed modes method with a static deflection shape was developed. This model was shown to be quite accurate, requiring only a few terms for accuracy comparable to that with hundreds of sine-only terms. Consequently, this control-oriented model facilitates low-order control design, evaluation and implementation. Several families of controllers for the active and semiactive devices were designed. Response of the passive and active systems were computed exactly via a Lyapunov equation, whereas semiactive system responses were computed using simulation.

A semiactive damper located 2% of the distance from the end of the cable, using a clipped optimal control algorithm with output feedback, weighting cable RMS displacement, was seen to decrease RMS responses to 63% lower than that of an optimal viscous damper, nearly the 76% achieved by fully active devices. Similar improvements may be observed at other damper locations. The equivalent modal damping of the first mode with a semiactive damper is significantly higher — about 8% of critical — than the optimal passive device, which can only add 1% damping for a damper location at $x_d = 0.02$. Thus, semiactive dampers have the potential to provide significantly improved mitigation of stay cable vibration.

There are several additional issues, such as the complexity of the cable model, not discussed herein that have been studied elsewhere. While the level of sag in cables of cable-stayed bridges is typically small (Irvine, 1981), passive damper performance is reduced some by cable sag (*e.g.*, Sulekh, 1990; Xu and Yu, 1998; Krenk and Nielsen, 2002); a study by the authors of the performance of semiactive damping for inclined flat-sag cables with axial flexibility is reported in Johnson *et al.*, (2003a). Additionally, Irvine (1981) also indicates that the flexural rigidity present in most cables is small, but cable bending stiffness is known to decrease the performance of the optimal passive damper; while this has not been extensively studied for semiactive control, the performance of active control was shown in Christenson (2001) to be relatively unaffected by

cable flexural rigidity. Christenson (2001) also investigates more realistic models of semiactive dampers, such as magnetorheological fluid dampers, for cable vibration mitigation. Finally, a laboratory experiment is discussed in Christenson (2001) and Christenson *et al.* (2006), and full-scale applications in Duan *et al.* (2005).

ACKNOWLEDGMENTS

The authors gratefully acknowledge the partial support of this research by the National Science Foundation, under grants CMS 95-00301, CMS 95-28083 and CMS 99-00234 (Dr. S.C. Liu, Program Director), and the LORD Corporation.

The genesis of this work occurred while Prof. Fujino was the visiting Melchor Chaired Professor of Civil Engineering at the University of Notre Dame, Fall 1997, and while Prof. Johnson was a Visiting Research Assistant Professor of Civil Engineering at the University of Notre Dame, Fall 1997 – Summer 1999.

APPENDIX I. COMPUTING EIGENFUNCTION ERROR

The relative error in the eigenfunctions is determined as follows. Assume the set of shape functions is given by

$$\phi_i(x) = \begin{cases} x/x_d, & i = 1, \quad 0 \leq x \leq x_d \\ (1-x)/(1-x_d), & i = 1, \quad x_d \leq x \leq 1 \\ \sin \pi(i-1)x & 1 < i \leq m \end{cases} \quad (42)$$

which includes the static deflection shape and the sinusoidal shapes. Let $\tilde{\phi}_i^m(x)$ denote the i^{th} eigenfunction computed using all m shape functions and $\tilde{\phi}_i^{q:r}(x)$ the i^{th} eigenfunction computed using a subset $\phi_q(x), \phi_{q+1}(x), \dots, \phi_r(x)$ of the shape functions. The error in the $\tilde{\phi}_i^{q:r}(x)$ eigenfunction, relative to $\tilde{\phi}_i^m(x)$, may be given by

$$\text{relative eigenfunction error} = \frac{\|\tilde{\phi}_i^{q:r}(x) - \tilde{\phi}_i^m(x)\|_2}{\|\tilde{\phi}_i^m(x)\|_2} \quad (43)$$

where the 2-norm is defined by

$$\|\cdot\|_2^2 = \int_0^1 |\cdot|^2 dx \quad (44)$$

One way to compute the integration in (44) is to discretize the shape functions at locations $x_j = j/n$, $j = 0, 1, \dots, n$, and use a vector norm. With a sufficiently large number of points, this should give reasonably accurate results. However, if few points are taken, or if large changes in slope occur between points (such as is seen in the cable/damper problem at $x = x_d$), significant error can be introduced into the computation of the relative eigenfunction error. Fortunately, computing the integral directly is not difficult, particularly since it turns out to involve elements of the mass matrix that had already been computed for solving for $\tilde{\phi}_i^m(x)$.

Let $\mathbf{M}^{q:r}$ denote the $(r-q+1) \times (r-q+1)$ portion of the $m \times m$ mass matrix \mathbf{M} given by rows q to r and columns q to r :

$$\begin{aligned} [\mathbf{M}^{q:r}]_{ij} &= m_{i+q-1, j+q-1}, & 1 \leq i \leq r-q+1, 1 \leq j \leq r-q+1 \\ [\mathbf{M}]_{ij} &= m_{ij} = \int_0^1 \phi_i(x) \phi_j(x) dx & 1 \leq i \leq m, 1 \leq j \leq m \end{aligned} \quad (45)$$

Also, let Φ_{ji}^m and $\Phi_{ji}^{q:r}$ denote the j^{th} row of the eigenvector (corresponding to mode i) of the state matrix computed using all m shape functions and the subset, respectively (*i.e.*, $\mathbf{A}\Phi^m = \Phi^m[\Lambda]$ where \mathbf{A} is as given in (20) using all m shape functions, and $\mathbf{A}^{q:r}\Phi^{q:r} = \Phi^{q:r}[\Lambda^{q:r}]$ where $\mathbf{A}^{q:r}$ is formed using $\mathbf{M}^{q:r}$ and similarly defined stiffness and damping matrices). Then the complex eigenfunctions are given by

$$\tilde{\phi}_i^m(x) = \sum_{j=1}^m \Phi_{ji}^m \phi_j(x) \quad \text{and} \quad \tilde{\phi}_i^{q:r}(x) = \sum_{j=1}^{r-q+1} \Phi_{ji}^{q:r} \phi_{j-1+q}(x) \quad (46)$$

The square of the norm of the difference between the two computed eigenfunctions is then

$$\begin{aligned} \|\tilde{\phi}_i^{q:r}(x) - \tilde{\phi}_i^m(x)\|_2^2 &= \int_0^1 |\tilde{\phi}_i^{q:r}(x) - \tilde{\phi}_i^m(x)|^2 dx \\ &= \int_0^1 [\tilde{\phi}_i^{q:r*}(x) \tilde{\phi}_i^{q:r}(x) - \tilde{\phi}_i^{q:r*}(x) \tilde{\phi}_i^m(x) - \tilde{\phi}_i^{q:r}(x) \tilde{\phi}_i^{m*}(x) + \tilde{\phi}_i^{m*}(x) \tilde{\phi}_i^m(x)] dx \\ &= \sum_{j=1}^{r-q+1} \sum_{k=1}^{r-q+1} \Phi_{ji}^{q:r*} \Phi_{ki}^{q:r} \int_0^1 \phi_{j-1+q}(x) \phi_{k-1+q}(x) dx \\ &\quad - \sum_{j=1}^{r-q+1} \sum_{k=1}^m \Phi_{ji}^{q:r*} \Phi_{ki}^m \int_0^1 \phi_{j-1+q}(x) \phi_k(x) dx \\ &\quad - \sum_{j=1}^m \sum_{k=1}^{r-q+1} \Phi_{ji}^{m*} \Phi_{ki}^{q:r} \int_0^1 \phi_j(x) \phi_{k-1+q}(x) dx \\ &\quad + \sum_{j=1}^m \sum_{k=1}^m \Phi_{ji}^{m*} \Phi_{ki}^m \int_0^1 \phi_j(x) \phi_k(x) dx \\ &= \sum_{j=1}^{r-q+1} \sum_{k=1}^{r-q+1} \Phi_{ji}^{q:r*} \Phi_{ki}^{q:r} m_{j-1+q, k-1+q} - \sum_{j=1}^{r-q+1} \sum_{k=1}^m \Phi_{ji}^{q:r*} \Phi_{ki}^m m_{j-1+q, k} \\ &\quad - \sum_{j=1}^m \sum_{k=1}^{r-q+1} \Phi_{ji}^{m*} \Phi_{ki}^{q:r} m_{j, k-1+q} + \sum_{j=1}^m \sum_{k=1}^m \Phi_{ji}^{m*} \Phi_{ki}^m m_{ij} \end{aligned} \quad (47)$$

where $(\cdot)^*$ denotes complex conjugate transpose. This simplifies quite nicely by using modified eigenvectors. Let \mathbf{v} and \mathbf{w} be $m \times 1$ vectors

$$\begin{aligned}\mathbf{v} &= [\Phi_{1i}^m \ \Phi_{2i}^m \ \dots \ \Phi_{mi}^m]^T \\ \mathbf{w} &= [\mathbf{0}_{1 \times (q-1)} \ \Phi_{1i}^{q:r} \ \Phi_{2i}^{q:r} \ \dots \ \Phi_{r-q+1,i}^{q:r} \ \mathbf{0}_{1 \times (m-r)}]^T\end{aligned}\quad (48)$$

Then (47) may be simplified as

$$\begin{aligned}\|\tilde{\phi}_i^{q:r}(x) - \tilde{\phi}_i^m(x)\|_2^2 &= \mathbf{w}^* \mathbf{M} \mathbf{w} + \mathbf{v}^* \mathbf{M} \mathbf{v} - \mathbf{w}^* \mathbf{M} \mathbf{v} - \mathbf{v}^* \mathbf{M} \mathbf{w} \\ &= [\mathbf{v} - \mathbf{w}]^* \mathbf{M} [\mathbf{v} - \mathbf{w}]\end{aligned}\quad (49)$$

The norm of the reference eigenfunction may be computed by replacing $\tilde{\phi}_i^{q:r}(x)$ by zero, which makes \mathbf{w} a zero vector, giving

$$\|\tilde{\phi}_i^m(x)\|_2^2 = \mathbf{v}^* \mathbf{M} \mathbf{v} \quad (50)$$

There is, however, one additional difficulty that can arise: the eigenvectors are unique only to within a (complex) scaling factor. Comparing the eigenfunctions computed with different sets of shape functions will require modifying one of the eigenfunctions by scaling and rotating in the complex plane before subtracting it from the reference computed eigenfunction. The difficulty here is how to do this scaling. One can attempt to scale by making the maximum deflection unity, but there may be discrepancies in where the two computed eigenfunctions have their peaks. One could also pick a specific location x_d at which to force the eigenfunctions to coincide, but if $\tilde{\phi}_i^{q:r}(x)$ happens to have its largest error at $x = x_d$, the scaling will bias the computed relative error. Consequently, the method used here is to find the complex scale factor that gives the smallest error.

Let J be the difference between the two eigenfunctions, where one is scaled by $(a + b\sqrt{-1})$,

$$\begin{aligned}J &= \|\tilde{\phi}_i^{q:r}(x) - \tilde{\phi}_i^m(x)\|_2^2 = [\mathbf{v} - (a + b\sqrt{-1})\mathbf{w}]^* \mathbf{M} [\mathbf{v} - (a + b\sqrt{-1})\mathbf{w}] \\ &= \mathbf{v}^* \mathbf{M} \mathbf{v} + a^2 \mathbf{w}^* \mathbf{M} \mathbf{w} - a[\mathbf{v}^* \mathbf{M} \mathbf{w} + \mathbf{w}^* \mathbf{M} \mathbf{v}] \\ &\quad + b^2 \mathbf{w}^* \mathbf{M} \mathbf{w} + b[\mathbf{w}^* \mathbf{M} \mathbf{v} - \mathbf{v}^* \mathbf{M} \mathbf{w}] \sqrt{-1}\end{aligned}\quad (51)$$

The “best” scaling will be the choice of a and b that minimize J . Setting to zero the partial derivatives of J with respect to a and b gives

$$\begin{aligned}\frac{\partial J}{\partial a} = 0 &= 2a\mathbf{w}^* \mathbf{M} \mathbf{w} - [\mathbf{v}^* \mathbf{M} \mathbf{w} + \mathbf{w}^* \mathbf{M} \mathbf{v}] \quad \Rightarrow \quad a = \frac{[\mathbf{v}^* \mathbf{M} \mathbf{w} + \mathbf{w}^* \mathbf{M} \mathbf{v}]}{2\mathbf{w}^* \mathbf{M} \mathbf{w}} = \frac{Re[\mathbf{w}^* \mathbf{M} \mathbf{v}]}{\mathbf{w}^* \mathbf{M} \mathbf{w}} \\ \frac{\partial J}{\partial b} = 0 &= 2b\mathbf{w}^* \mathbf{M} \mathbf{w} + [\mathbf{w}^* \mathbf{M} \mathbf{v} - \mathbf{v}^* \mathbf{M} \mathbf{w}] \sqrt{-1} \quad \Rightarrow \quad b = \frac{[\mathbf{w}^* \mathbf{M} \mathbf{v} - \mathbf{v}^* \mathbf{M} \mathbf{w}]}{2\mathbf{w}^* \mathbf{M} \mathbf{w} \sqrt{-1}} = \frac{Im[\mathbf{w}^* \mathbf{M} \mathbf{v}]}{\mathbf{w}^* \mathbf{M} \mathbf{w}}\end{aligned}\quad (52)$$

The scale factor, then, is $(a + b\sqrt{-1}) = (\mathbf{w}^* \mathbf{M} \mathbf{v}) / (\mathbf{w}^* \mathbf{M} \mathbf{w})$. Substituting back into (51) and simplifying gives

$$\|\tilde{\phi}_i^{q:r}(x) - \tilde{\phi}_i^m(x)\|_2^2 = \frac{\mathbf{v}^* \mathbf{M} [\mathbf{v} \mathbf{w}^T - \mathbf{w} \mathbf{v}^T] \mathbf{M} (\mathbf{w}^*)^T}{\mathbf{w}^* \mathbf{M} \mathbf{w}} \quad (53)$$

Finally, the relative eigenfunction error may be given as

$$\frac{\|\tilde{\phi}_i^{q:r}(x) - \tilde{\phi}_i^m(x)\|_2}{\|\tilde{\phi}_i^m(x)\|_2} = \left\{ \frac{\mathbf{v}^* \mathbf{M} [\mathbf{v} \mathbf{w}^T - \mathbf{w} \mathbf{v}^T] \mathbf{M} (\mathbf{w}^*)^T}{\mathbf{w}^* \mathbf{M} \mathbf{w} \mathbf{v}^* \mathbf{M} \mathbf{v}} \right\}^{1/2} \quad (54)$$

APPENDIX II. ESTIMATE OF SEMIACTIVE DAMPING FORCES IN FULL-SCALE

In design of an actual damper, nominal damper force levels should be estimated so that an appropriate damper design force level can be implemented. To get an idea of the typical force level required to semiactively control a stay cable on an actual bridge, a stay cable from one bridge is examined. Rain-wind induced cable vibration on the Aratsu Bridge in Fukuoka, Japan, has been observed to cause peak-to-peak cable deflections of 60 cm (Yoshimura *et al.*, 1989). One particular cable on this bridge is 92.28 m long and carries a tension of 3.0 MN (Pacheco *et al.*, 1993). Assume this cable is excited by a zero mean Gaussian white noise excitation multiplied by the first sinusoidal mode shape that results in a 30 cm amplitude deflection at the center of the cable. The peak control forces required for this deflection are computed.

Assume that the ratio of peak displacement to RMS displacement is on the order of 2. (The factor of 2 is somewhere between the factor of $1/\sqrt{2}$ for a sinusoidal signal and the $1/3$ typical of Gaussian processes.) Thus, it is assumed that the uncontrolled RMS displacement at the center of the cable is on the order of 15 cm. With a semiactive damper at $x_d = 0.02$, controlled with displacement weighting with a control weight chosen for small cable displacement, 1% sensor noise using a Kalman filter, this same excitation would cause the RMS damper force to be a nondimensional 0.8697×10^{-3} , corresponding to a dimensional RMS force of 25.8 kN (5.8 kip). If the RMS force of the damper is a zero mean process, as with the ideal device assumed here, then the peak damper force may be approximated as twice the RMS, giving about a 52 kN (12 kip) force to add 8% equivalent damping to reduce the cable response by about 89% compared to an uncontrolled cable with about 0.1% damping, or by about 64% compared to the same cable with the ideal passive damper providing 1.0% damping (which uses peak forces about 8 kN). These force levels are for a fairly aggressive controller; a less-aggressive semiactive controller can add an 5.7% equivalent damping to reduce the uncontrolled response by 86.5% (57.5% relative to the ideal passive) by using a peak force only 18.8 kN (4.2 kip).

This estimate is admittedly quite rough, but gives an order-of-magnitude approximation of the required damper forces. Yoshimura *et al.* (1989) and Pacheco *et al.* (1993) do not specify which cable on this bridge had the 60 cm peak-to-peak displacements, so the force estimate here may be higher or lower accordingly. Additionally, the true wind/rain excitation mechanism is complex and likely quite different from that used here. Regardless, this exercise gives some measure of confidence that the damper force levels are reasonable and are well within the capabilities of the current state-of-the art in semiactive devices (Spencer and Sain, 1997).

APPENDIX III. REFERENCES

- Craig, R., Jr. (1981). *Structural Dynamics: An Introduction to Computer Methods*, John Wiley & Sons, New York, 350–353.
- Christenson, R.E. (2001). “Semiactive Control of Civil Structures for Natural Hazard Mitigation: Analytical and Experimental Studies.” Ph.D. dissertation, University of Notre Dame, Notre Dame, Indiana.

- Christenson, R.E., Spencer, B.F., Jr., and Johnson, E.A. (2006). "Experimental Verification of Smart Cable Damping." *Journal of Engineering Mechanics*, ASCE, **132**(3), 268–278.
- Duan, Y.F., Ni, Y.Q., and Ko, J.M. (2005). "State-Derivative Feedback Control of Cable Vibration using Semiactive Magnetorheological Dampers." *Computer-Aided Civil and Infrastructure Engineering*, **20**(6), 431–449.
- Dyke, S.J., Spencer, B.F., Jr., Sain, M.K., and Carlson, J.D. (1996a). "Seismic Response Reduction Using Magnetorheological Dampers." *Proc. IFAC World Congress*, San Francisco, CA, Vol. L, 145–150.
- Dyke, S.J., Spencer, B.F., Jr., Sain, M.K., and Carlson, J.D. (1996b). "Modeling and Control of Magnetorheological Dampers for Seismic Response Reduction." *Smart Materials and Struct.*, **5**(5), 565–575.
- Endo, T., Iijima, T., Okukawa, A., and Ito, M. (1991). "The Technical Challenge of a Long Cable-Stayed Bridge — Tatara Bridge". In M. Ito, Y. Fujino, T. Miyata, and N. Narita (eds.), *Cable-stayed Bridges — Recent Developments and their Future*, Elsevier, 417–436.
- Fujino, Y., Soong, T.T., and Spencer, B.F., Jr. (1996). "Structural Control: Basic Concepts and Applications." *Proceedings of the ASCE Structures Congress XIV*, Chicago, Illinois, April 15–18, 1996, 1277–1287.
- Fujino, Y., Warnitchai, P., and Pacheco, B.M. (1993). "Active Stiffness Control of Cable Vibration." *Journal of Applied Mechanics*, ASME, **60**(4), 948–953.
- Gimsing, N.J. (1983). *Cable-Supported Bridges*, John Wiley & Sons, Chichester, England.
- Hikami, Y. (1986). "Rain Vibrations of Cables of Cable Stayed Bridge." *Journal of Wind Engineering*, JAWE, no. 27, 17–28 (in Japanese).
- Hikami, Y. and Shiraishi, N. (1988). "Rain-Induced Vibrations of Cables in Cable-Stayed Bridges." *Journal of Wind Engineering and Industrial Aerodynamics*, **29**(1–3), 409–418.
- Housner, G.W., Bergman, L.A., Caughey, T.K., Chassiakos, A.G., Claus, R.O., Masri, S.F., Skelton, R.E., Soong, T.T., Spencer, B.F., Jr., and Yao, J.T.P. (1997). "Structural Control: Past and Present." *Journal of Engineering Mechanics*, ASCE, **123**(9), 897–971.
- Irvine, H.M. (1981). *Cable Structures*, MIT Press, Cambridge, Massachusetts.
- Johnson, E.A., Ramallo, J.C., Spencer, B.F., Jr., and Sain, M.K. (1999a). "Intelligent Base Isolation Systems." *Proc. Second World Conf. on Struct. Control*, Kyoto, Japan, Vol.1, 367–376. Draft version available online at http://rcf.usc.edu/~johnsone/papers/smartbaseiso_2wsc.html
- Johnson, E.A., Baker, G.A., Spencer, B.F., Jr., and Fujino, Y. (2007). "Semiactive Damping of Stay Cables." *Journal of Engineering Mechanics*, ASCE, **133**(1), in press. Draft version available online at http://rcf.usc.edu/~johnsone/papers/smartdamping_tautcable_jem.html
- Johnson, E.A., Christenson, R.E., and Spencer, B.F., Jr. (2003). "Semiactive Damping of Cables with Sag." *Computer Aided Civil and Infrastructure Engineering*, **18**(2), 132–146. Draft version available online at http://rcf.usc.edu/~johnsone/papers/smartdamping_sagcable.html
- Johnson, E.A., Spencer, B.F., Jr., and Fujino, Y. (1999b). "Semiactive Damping of Stay Cables: A Preliminary Study." *Proceedings of the 17th International Modal Analysis Conference (IMAC XVII)*, Society for Experimental Mechanics, Bethel, Connecticut, 417–423.
- Kovacs, I. (1982). "Zur Frage der Seilschwingungen und der Seildämpfung." *Die Bautechnik*, **59**(10), 325–332, (in German).
- Krenk, S. (2000). "Vibrations of a Taut Cable with an External Damper." *Journal of Applied Mechanics*, ASME, **67**(4), 772–776.
- Krenk, S., and Nielsen, S.R.K. (2002). "Vibrations of a Shallow Cable with a Viscous Damper." *Proceedings of the Royal Society of London, Ser. A*, **458**(2018), 339–357.
- Krenk, S., and Høgsberg, J.R. (2005). "Damping of Cables by a Transverse Force." *Journal of Engineering Mechanics*, ASCE, **131**(4), 340–348.
- Main, J.A. and Jones, N.P. (1999). "Full-Scale Measurements of Stay Cable Vibration." In A. Larsen, G.L. Larose and F.M. Livesey (eds.), *Wind Engineering into the 21st Century*, Balkema, Rotterdam, 963–970.
- Main, J.A., and Jones, N.P. (2002a). "Free Vibrations of Taut Cable with Attached Damper. I: Linear Viscous Damper." *Journal of Engineering Mechanics*, ASCE, **128**(10), 1062–1071.
- Main, J.A., and Jones, N.P. (2002b). "Free Vibrations of Taut Cable with Attached Damper. II: Nonlinear Damper." *Journal of Engineering Mechanics*, ASCE, **128**(10), 1072–1081.
- Matsumoto, M. (1998). "Observed Behavior of Prototype Cable Vibration and its Generation Mechanism." In A. Larsen and S. Eisdahl, eds., *Bridge Aerodynamics*, Balkema, Rotterdam, 189–211.
- Pacheco, B.M., Fujino, Y., and Sulekh, A. (1993). "Estimation Curve for Modal Damping in Stay Cables with Viscous Damper." *Journal of Structural Engineering*, ASCE, **119**(6), 1961–1979.

- Poston, R.W. (1998). "Cable-Stay Conundrum." *Civil Engineering*, **68**(8), 58–61.
- Russell, H. (1999). "Hong Kong Bids for Cable-Stayed Bridge Record." *Bridge Design and Engineering*, No. 15 (second quarter), 7.
- Scanlon, R.H. (1999). Personal communication with Erik A. Johnson, February 22, 1999.
- Spencer, B.F., Jr., Dyke, S.J., Sain, M.K., and Carlson, J.D. (1997). "Phenomenological Model for Magnetorheological Dampers." *ASCE Journal of Engineering Mechanics*, **123**(3), 230–238.
- Spencer, B.F., Jr. and Sain, M.K. (1997). "Controlling Buildings: A New Frontier in Feedback." *IEEE Control Systems Magazine*, **17**(6), 19–35. Draft version available online at <http://cee.uiuc.edu/sstl/CSM.html>
- Stengel, R.F. (1986). *Stochastic Optimal Control: Theory and Application*, John Wiley & Sons, New York.
- Sulekh, A. (1990). *Non-dimensionalized Curves for Modal Damping in Stay Cables with Viscous Dampers*, Master's Thesis, Department of Civil Engineering, University of Tokyo, Tokyo, Japan.
- Virloguex, M., et al. (1994). "Design of the Normandie Bridge". *Proceedings of the International Conference on Cable-Stayed and Suspension Bridges*, IABSE, Deauville, France, Vol. 1, 605–630.
- Watson, S.C. and Stafford, D. (1988). "Cables in Trouble." *Civil Engineering*, ASCE, **58**(4), 38–41.
- Xu, Y.L., and Yu, Z. (1998). "Vibration of Inclined Sag Cables with Oil Dampers in Cable-Stayed Bridges." *Journal of Bridge Engineering*, **3**(4), 194–203.
- Yamaguchi, H. and Dung, N.N. (1992). "Active Wave Control of Saggged-Cable Vibration." *Proceedings of the First International Conference on Motion Vibration Control*, Yokohama, Japan, 134–139.
- Yamaguchi, H. and Fujino, Y. (1998). "Stayed Cable Dynamics and its Vibration Control." In A. Larsen and S. Eisdahl, eds., *Bridge Aerodynamics*, Balkema, Rotterdam, 235–253.
- Yang, G., Spencer, B.F., Jr., Carlson, J.D., and Sain, M. K. (2002). "Large-scale MR Fluid Dampers: Modeling and Dynamic Performance Considerations." *Engineering Structures*, **24**(3), 309–323.
- Yoshimura, T., Inoue, A., Kaji, K., and Savage, M. (1989). "A Study on the Aerodynamic Stability of the Aratsu Bridge." *Proceedings of the Canada-Japan Workshop on Bridge Aerodynamics*, Ottawa, Canada, 41–50.

APPENDIX IV. NOTATION

The following symbols are used in this paper:

$()', ()$	partial derivatives with respect to x and t
$(\bar{\cdot})$	dimensional quantity
$(\cdot)^*$	complex conjugate transpose
$\ \cdot\ _2$	eigenfunction L_2 norm
$\mathbf{0}$	matrix of zeros
$\mathbf{A}, \mathbf{B}, \mathbf{G}$	matrices in state equation
$\mathbf{A}_{\text{KF}}, \mathbf{B}_{\text{KF}}, \mathbf{G}_{\text{KF}}$	estimator state equation matrices
$(a + b\sqrt{-1})$	eigenfunction scaling factor (used in computing eigenfunction errors)
c	cable damping per unit length
c_d	viscous damping coefficient of attached passive linear viscous damper
$\mathbf{C}_z, \mathbf{D}_z, \mathbf{H}_z$	matrices in regulated outputs equation
$\mathbf{C}_y, \mathbf{D}_y, \mathbf{H}_y$	matrices in sensor equation
$\mathbf{A}_p, \mathbf{C}_p$	modified state and output matrices for passive damper
$E[\cdot]$	expectation operator
$F_d^{\text{active}}(t)$	force commanded by primary controller

f_i, \mathbf{f}	external load coefficient on i^{th} generalized displacement, external load vector
$f(x, t)$	external distributed load on the cable
\mathbf{I}	identity matrix
J_k	k^{th} cost function
L, T, ρ	cable length, tension, mass per unit length (dimensional)
\mathbf{L}_k	state feedback gain for the k^{th} cost function
\mathbf{L}_{KF}	Kalman filter estimator gain
$\mathbf{M}, \mathbf{C}, \mathbf{K}$	mass, damping, and stiffness matrices
$\mathbf{M}^{1/2}$	matrix square root of the mass matrix; <i>i.e.</i> , $\mathbf{M}^{1/2}\mathbf{M}^{1/2} = \mathbf{M}$
$\mathbf{M}^{q:r}$	a portion (rows and columns q to r) of the mass matrix
m	number of shape functions used in expansion of $v(x, t)$
m_{ij}, c_{ij}, k_{ij}	elements of mass, damping, and stiffness matrices
$\tilde{\mathbf{P}}$	solution to estimator algebraic Riccati equation
\mathbf{P}_k	solution to control design algebraic Riccati equation
\mathbf{Q}_k	weight on output for the k^{th} cost function
$\mathbf{Q}_{\text{KF}}, \mathbf{R}_{\text{KF}}$	covariance (or spectral density magnitude) of excitation and sensor noise
$q_i(t), \mathbf{q}(t)$	i^{th} generalized displacement and generalized displacement vector
R	control weight in cost function
\mathbf{S}_0	excitation spectral density magnitude matrix
\mathbf{v}	sensor noise vector
\mathbf{v}, \mathbf{w}	modified eigenvectors used in computing eigenfunction errors
$v(x, t)$	transverse deflection of the cable
$v(x_d, t), \ddot{v}(x_d, t)$	displacement and acceleration at the damper location
$\dot{v}(x_d, t), \dot{v}_d$	velocity at the damper location
$W(t)$	zero-mean Gaussian white noise excitation process
$x_d, F_d(t)$	damper location and its force
\mathbf{y}	vector of noisy sensor measurements
\mathbf{z}	vector of generalized coordinates and their derivatives $[\mathbf{q}^T \quad \dot{\mathbf{q}}^T \quad \ddot{\mathbf{q}}^T]^T$
$\alpha_i(x), \boldsymbol{\beta}(t)$	variables used in expansion of external distributed load
$\alpha(\dot{v})$	force modulation function
$\delta(\cdot)$	Dirac delta function
δ_{ij}	Kronecker delta
$\boldsymbol{\eta}$	state vector $[\mathbf{q}^T \quad \dot{\mathbf{q}}^T]^T$
$\hat{\boldsymbol{\eta}}$	estimate of the state vector $\boldsymbol{\eta}$
$\boldsymbol{\Sigma}$	the solution to a Lyapunov equation

$\sigma_{\text{acceleration}}$	RMS cable acceleration
$\sigma_{\text{displacement}}$	RMS cable displacement
σ_{velocity}	RMS cable velocity
Φ_{ji}^m	j^{th} row of i^{th} eigenvector computed using first m shape functions
$\Phi_{ji}^{q:r}$	j^{th} row of i^{th} eigenvector computed using subset of shape functions
$\phi_i(x), \Phi(x)$	i^{th} shape function and shape function vector
$\tilde{\phi}_i^m(x)$	i^{th} mode computed using m shape functions
$\tilde{\phi}_i^{499s+sd}(x)$	i^{th} mode computed using 499 sine shapes plus the static deflection shape
$\tilde{\phi}_i^{q:r}(x)$	i^{th} eigenfunction computed using subset $\phi_q(x), \dots, \phi_r(x)$ of the shape functions
φ_i, Φ	damper load coefficient on i^{th} generalized displacement, damper load vector
ω_0	fundamental natural frequency of the undamped cable
$\omega_i, \zeta_i, \tilde{\phi}_i(x)$	natural frequency, damping ratio, and eigenfunction of the i^{th} mode